Copyright Warning & Restrictions

The copyright law of the United States (Title 17, United States Code) governs the making of photocopies or other reproductions of copyrighted material.

Under certain conditions specified in the law, libraries and archives are authorized to furnish a photocopy or other reproduction. One of these specified conditions is that the photocopy or reproduction is not to be "used for any purpose other than private study, scholarship, or research." If a, user makes a request for, or later uses, a photocopy or reproduction for purposes in excess of "fair use" that user may be liable for copyright infringement,

This institution reserves the right to refuse to accept a copying order if, in its judgment, fulfillment of the order would involve violation of copyright law.

Please Note: The author retains the copyright while the New Jersey Institute of Technology reserves the right to distribute this thesis or dissertation

Printing note: If you do not wish to print this page, then select "Pages from: first page # to: last page #" on the print dialog screen

ABSTRACT

SYNTHESIS AND CHARACTERIZATION OF PHOSPHOSILICATE GLASS THIN FILMS FOR SENSOR APPLICATION

by
Hui Wu

This study was dedicated to the synthesis of the thin film materials required to fabricate the waveguide and the reference arm barrier for integrated optical sensor. Phosphosilicate glass (PSG) thin films were synthesized on silicon and quartz wafers by LPCVD using Ditertiarybutylsilane(DTBS), Trimethylphosphite(TMP) and oxygen as precursors. The films were processed at different temperatures between 600°C and 700°C at a constant pressure, and at different flow rate of TMP.

The effect of TMP flow rate and deposition temperature on deposition parameters and the properties of PSG films were investigated. The films deposited were uniform, amorphous, low stress and the composition of the films varied with deposition temperature and TMP flow rate. The deposition rate increased with increasing TMP flow rate and had a maximum of deposition rate at 650 ^{0}C. It was suggested that the addition of TMP catalyzes the deposition. Refractive index increased with increasing deposition temperature and phosphorus concentration. A less transparent film at higher temperatures also suggested presence of carbon at higher temperatures, This may be due to a possible decomposition reaction of TMP or DTBS. The PSG films showed around 100% transparency when deposited at 650 ^{0}C.

SYNTHESIS AND CHARACTERIZATION OF PHOSPHOSILICATE GLASS FILMS BY LPCVD FOR SENSOR APPLICATION

by

Hui Wu

A Thesis
Submitted to the Faculty of
New Jersey Institute of Technology
in Partial Fulfillment of the Requirements for the Degree of
Master of Science in Engineering Science

Interdisciplinary Program in Materials Science and Engineering

October 1997

APPROVAL PAGE

SYNTHESIS AND CHARACTERIZATION OF PHOSPHOSILICATE GLASS FILMS FOR SENSOR APPLICATION

Hui Wu

Dr. Roland A. Levy, Thesis Advisor — Date
Professor of Physics,
Director of Materials Science and Engineering Program, NJIT

Dr. John Frederici — Date
Professor of Physics, NJIT

Dr. Lev N. Krasnoperov — Date
Professor of Chemical Engineering, Chemistry, and
Environmental Science, NJIT

BIOGRAPHICAL SKETCH

Author: Hui Wu

Degree: Master of Science

Date: October, 1997

Undergraduate and Graduate Education:

- Master of Science in Engineering Science,
  New Jersey Institute of Technology,
  Newark, New Jersey, 1997

- Master of Science in Engineering Science
  Shanghai Institute of Metallurgy, Chinese Sciences and Academy
  Shanghai, China, 1994

- Bachelor of Science in Materials Science and Engineering
  Zhejiang University,
  Hangzhou, China, 1991

Major: Materials Science and Engineering

This thesis is dedicated to
my beloved family

ACKNOWLEDGMENT

The author expresses his sincere gratitude to his advisor, Professor Roland A. Levy for his guidance, inspiration, and support throughout this research.

Special thanks to Professor Vladimir B. Zaitsev, Professor John Federici, and Professor Lev N. Krasnoperov for serving as members of the thesis review committee.

The author appreciates the timely help and suggestion from the CVD laboratory members, including: Vitaly Sigal, Dr. Jan Opyrchal, Dr. Romiana Petrova, Dr. Vladimir B. Zaitsev, Dr.Sergey Korenev, Krit Aryusook, Wiriya Thongruang, Sutham Niyomwas, Chenna Ravindranath, Muhammad A. Hussain, Ramanuja Narahari, Oleg Mitrofanov.

TABLE OF CONTENTS

Chapter	Page
1 INTRODUCTION	1
1.1 Research Background	1
1.2 The Mechanism of Mach-Zehnder Interferometer	3
1.3 Flow Sheet for Fabrication of Mach-Zehnder Interferometer	7
1.4 The Objective of this Study	9
2 REVIEW OF LITERATURE	10
2.1 Deposition Techniques	10
2.1.1 The Advantages of LPCVD	10
2.1.2 LPCVD of Undoped and Doped Silicon Dioxide	12
2.2 Properties of Undoped and P-doped Silicon Dioxide Films	14
2.2.1 Undoped Silicon Dioxide Films	14
2.2.2 Phosphosilicate Glass	16
2.3 Phosphosilicate Glass	16
2.3.1 PSG Water Absorption and PSG Structure	16
2.3.2 Reflow of PSG	17
2.3.3 Phosphorus Concentration and its Measurement	18
2.4 Previous Work for this Project	21
3 EXPERIMENTAL SETUP AND CHARACTERIZATION TECHNIQUES	23
3.1 Introduction	23
3.2 Deposition	23
3.2.1 Experimental Setup	23
3.2.2 Deposition Procedure	29
3.3 Characterization of Phosphosilicate Glass	30
3.3.1 Thickness	30

TABLE OF CONTENTS
(Continued)

Chapter	Page
3.3.2 Refractive Index	31
3.3.3 Infrared Spectra	31
3.3.4 Stress	32
3.3.5 Optical Transmission	33
4 RESULTS AND DISCUSSION	34
4.1 Introduction	34
4.2 Deposition of PSG	34
4.2.1 The Effect of Wafer to Wafer Space	34
4.2.2 The Effect of TMP Flow Rate and Temperature on Deposition Rate	34
4.2.3 The Effect of TMP Flow Rate and Temperature on Uniformity	38
4.2.4 The Effect of TMP Flow Rate and Temperature on Concentration	40
4.3 Physicochemical Properties of PSG Films	43
4.3.1 The Density of PSG Films	43
4.3.2 The Stress of PSG Films	44
4.3.3 Refractive Index of PSG Films	46
4.3.4 Optical Transparency of PSG Films	47
5 CONCLUSIONS	52
REFERENCES	54

LIST OF TABLES

Table	Page
2.1 Properties of Thermal Silicon Dioxide	15
3.1 Specifications of the Si wafer	24

LIST OF FIGURES

Figure		Page
1.1	Schematic representation of sensor system	2
1.2	Schematic of interferometer with two Y-splitter	4
2.1	The schematic of FTIR analysis	21
3.1	A Schematic of the LPCVD reactor	26
4.1	PSG growth rate vs. TMP flow rate, DTBS/Oxygen=1:15	35
4.2	The Effect of temperature on growth rate of PSG, DTBS:Oxygen:TMP=2:30:1	36
4.3	Depletion vs. TMP flow rate, DTBS/oxygen=1:15	37
4.4	The depletion of PSG vs. temperature, DTBS:Oxygen:TMP=2:30:1	37
4.5	Thickness variation vs. TMP flow rate, DTBS/Oxygen=1:15	39
4.6	Thickness variation vs. Temperature, DTBS:Oxygen:TMP=2:30:1	39
4.7	FTIR results at different position across the same wafer Flow rate ratio is DTBS:Oxygen:TMP=10:150:7	40
4.8	The Effect of TMP flow rate on phosphorus oxide concentration DTBS/Oxygen=1:15	41
4.9	The Effect of deposition temperature on phosphorus oxide concentration DTBS:Oxygen:TMP=2:30:1	41
4.10	The density of PSG vs TMP flow rate DTBS:Oxygen=1:15	43
4.11	The effect of temperature on density, DTBS:Oxygen:TMP=2:30:1	44
4.12	Stress of PSG films vs TMP flow rate, DTBS/Oxygen=1:15	45
4.13	Stress of PSG films at different temperature, DTBS:Oxygen:TMP=2:30:1	45
4.14	Refractive Index vs TMP flow rate, DTBS/Oxygen=1:15	48

LIST OF FIGURES
(Continued)

Figure **Page**

4.15 The effect of temperature on refractive index of PSG, DTBS:Oxygen:TMP=2:30:1 48

4:16 Transmission of PSG deposited at different TMP flow rate, DTBS/Oxygen=1:15, Deposition temperature: 700 ^{0}C 49

4.17 Transmission of PSG deposited at different temperature, DTBS:Oxygen:TMP=2:30:1 49

4.18 FTIR results at different temperature, (a) 700 ^{0}C (b) 650 ^{0}C (c) 600 ^{0}C 50

absorptions in the near infrared (1500-1900nm) which attenuates the light propagating along the fiber optic cable. By measuring the transmission of broadbanded light through the fiber and matching the recorded spectrum to known standards, the composition and concentration of the pollutants can be determined.

In an ongoing research program in NJIT, we combine both the interferometric and evanescent wave techniques into a single compact sensor technology capable of measuring several pollutants simultaneously. Therefore, this proposed sensor is essentially a Mach-Zehnder interferometer with sampling capabilities over a large wavelength range (1000-1900nm). The use of such a sensor permits a shorter active sampling length (~0.5 cm)as compared to evanescent wave fiber optic sensors (1-10m) due to the inherent sensitivity of interferometric detection. By using a broadbanded light source rather than a single wavelength laser, the interferometer can measure the refractive index difference over the entire near infrared spectrum. This proposed detection system would consist of a bright broadbanded light source, a coupling lens, optical fibers, the IOS(Insulator On Silicon), and an optical spectrum analyser (Fig.1.1).

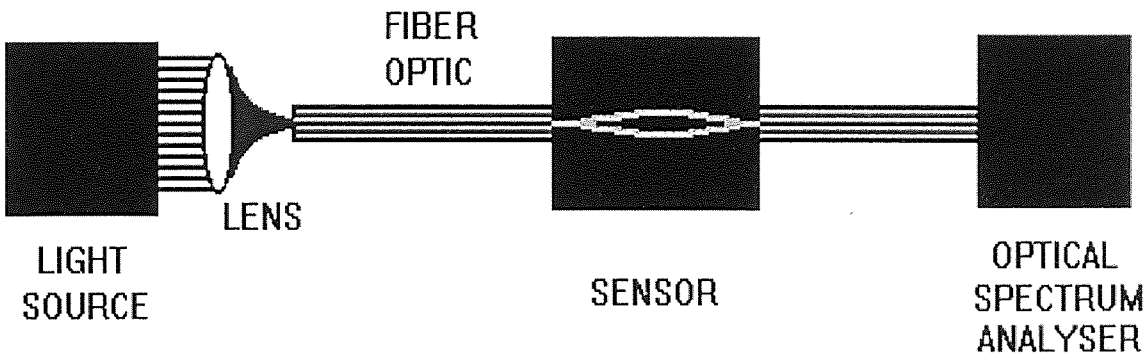

Fig.1.1 Schematic representation of sensor system

An important advantage of this sensor is its size. The distance between the interferometer's arms is on the order of 0.1 mm while the length of the interferometer is on the order of 1 cm. By placing numerous interferometers parallel to each other with different coatings, the resultant device can be made to measure the concentration of different pollutant species simultaneously. The area of the device occupies an area no bigger than a thumb nail. Another advantage to this approach is the compatibility of the technology with standard silicon-based processing where photolithography and chemical etching steps can be used to mass produce copies of the pattern at a cost of less than a dollar per chip. The use of fiber optics for coupling light in and out of the interferometer offers the additional advantage of remote sensing in environment. For a typical arm length L = 0.6 cm, and a λ_o = 633 nm, $\Delta\Phi = \pi$ (i.e.,1 fringe shift or 100% signal modulation) for a $\Delta n_{eff} = 6x10^{-5}$. Therefore, extremely small changes in the effective index, caused by low concentrations of pollutants (as low as 1 ppb) in the water, can be measured using this interferometric approach.

This proposed sensor system is compact, portable, and non-intrusive. It is expected to provide accurate, real time, and cost effective monitoring and characterization of pollutants in water or air systems.

1.2 The Mechanism of Integrated Optical Sensor

The integrated optical sensor combines the properites of Mach-Zehnder interferometer and evanescent wave absorption spectroscopy. The operation of the Mach-Zehnder interferometric sensor is based on the detection of changes in the refractive index from baseline value due to the presence of pollutants [7]. These changes are measured by

exposing one arm of a symmetric Mach-Zehnder interferometer to the contaminated liquid while the other reference arm is being protected by a glass buffer layer. The interferometric output can be calculated as a function of arm length and index difference between the reference and the active arm.

Fig.1.2 Schematic of interferometer with two Y-splitter

Laser light is coupled into the waveguide and split into the reference and sampling arms using a Y-splitter configuration (Fig.1.2). When the active arm is exposed to pollutant molecules, there is an effective change in the refractive index sampled by that arm. Thickness changes can also occur in any hydrophobic layer which adheres to the coated arm affecting the refractive index sampled by that arm. Therefore, a phase difference, $\Delta\Phi$, develops between the active and reference arm. When light from the two interferometer arms recombine, constructive or destructive interference occurs and the light intensity exiting the interferometer, I_x, ratioed to input light. I_o, is given by :

$$I_x/I_o = 1/2\ (1 + \cos \Delta\Phi)$$

where

$$\Delta\Phi = 2\pi L(n_2-n_1)/\lambda_o$$

with L being the common length for both arms of the interferometer, n_i the effective index of arm i, and λ_o is the input light wavelength. Therefore, the phase difference is

directly proportional to the effective index difference ($\Delta n_{eff} = n_2 - n_1$) between the waveguide arms. Since the pollutant level affects Δn_{eff}, then the interferometer's output intensity changes with the concentration of pollution present in the sample.

However, by using a broadband light source, rather than a single wavelength laser, the interferometer can measure the refractive index difference and absorption of the evanescent wave over a wide spectrum.

The theory of evanescent wave absorption spectroscopy (EWAS) has been extensively reported [8]. Useful from the UV-visible to mid-IR spectral region, it is fundamentally the same as attenuated total reflection (ATR). However, in ATR, light strikes the interface between waveguide and sample at a single angle. In EWAS, where the waveguide is essentially a fiber optic, there exists a range of incident angles. Upon total internal reflection of light in the waveguide, a portion of light enters the surrounding medium. This is known as the evanescent wave. Its depth of penetration, d_p, defined as the depth where light intensity is reduced to 1/e of its value at the interface, can be expressed as

$$d_p = \frac{\lambda_1}{2\pi(\sin^2\theta - n^2)^{1/2}}$$

where θ is the angle of incidence at the interface with respect to the normal; λ_1 is the wavelength of light in the waveguide medium, λ/n_1; and n is the refractive index ratio of the waveguide and surrounding medium, n_1/n_2. For a fiber optic, this represents the core-to-cladding refractive index ratio.

$$-\log(I/I_0) = \alpha_e Lc + 2\cdot\log(NA_0/NA)$$

where I is the transmitted light intensity after sensor exposure to analyte, I_0 is a reference intensity with no analyte present, L is a sensor length, c is a molar concentration, and NA and NA_0 are the sensor numerical apertures with and without analyte present, respectively. The numerical aperture, NA, determines the amount of light collected by the fiber from an infinite source. It is defined as

$$NA = n_{ext}\sin\theta_a = \sqrt{(n_1 + n_2)\cdot(n_1 - n_2)}$$

where n_{ext} is the refractive index of the external medium and is the θ_a acceptance angle of the fiber. The effective molar absorptivity, α_e is defined as

$$\alpha_e = \varepsilon\eta_p$$

where ε is the molar absorptivity of the infrared active species, and η_p, the fraction of light entering the fiber present in the cladding, is expressed as

$$\eta_p = k/V$$

where k is a proportionality constant, determined by Gloge[23] to be 1.89 for equilibrium mode distribution in a fiber. The denominator in Eq. 7 is known as the V parameter. It determines the number of optical modes a fiber can support and is defined as

$$V = \frac{2\pi R\sqrt{(n_1 + n_2)\cdot(n_1 - n_2)}}{\lambda}$$

where R is the radius of the fiber core.

In general the two terms on the right-hand side of equation can be described, from left to right, respectively, as a Beer's law relationship where attenuation is due to absorption of light by infrared-active species, as well as a light-guiding relationship dependent on the refractive index of core and cladding.

Our choice of materials for the case, core and cladding layers of the waveguides was dictated by materials readily available in the silicon industry. Silicon dioxide films containing small amount of phosphorus could be used to build the optical fiber for the integrated device since the difference between its refractive index and that of silicon dioxide is small enough for total internal reflection., and the difference of refractive index can be designed by controlling the phosphorus content. The phosphosilicate glass has been used for fabricating optical ring resonators where channel waveguide losses of 1dB/cm at visible wavelengths have been obtained [9].

1.3 Flow Sheet for Fabrication of Integrated Optical Sensor

Silicon Wafer

↓

Deposition of Pad oxide

↓

Deposition of Silicon nitride

(acts as a mask for definition of windows)

↓

Photolithography (V-Grooves)

↓

Reactive Ion Etching(RIE) of silicon nitride

↓

Removal of pad oxide

↓

Wet Etching of wafer in 49% KOH to get V Grooves

↓

Removal of silicon nitride

↓

Deposition of 10μm oxide

(to prevent light from being absorbed by the Si)

↓

Deposition of P Glass(~4μm)

(core layer of the waveguide)

↓

Photolithography of P Glass

(to get the arms of the interferometer)

↓

Reactive Ion Etching (RIE) of P Glass

↓

Deposition of Oxide layer(~2μm)

(cladding layer for the waveguide)

↓

Photolithography of Oxide

(to form the cladding over the reference arm)

↓

Reactive Ion Etching (RIE) of Oxide

1.4 The Objective of this Study

This study did not focus on the actual fabrication of the interferometer, it laid the foundation for the fabrication of the interferometer — the synthesis of the thin film materials required to fabricate the waveguide and the reference arm barrier. Here, the main concern is put on the deposition of the core material—PSG. LPCVD processes were developed to produce uniform, low stress and transparent phosphorus-doped silicon dioxide films.

CHAPTER 2

REVIEW OF LITERATURE

In this chapter, LPCVD and PSG deposition will be reviewed first. Then a review of properties of PSG and its concentration measurement will be discussed.

2.1 Deposition Techniques

Chemical Vapor Deposition (CVD) is one of the most important methods of film formation used in the fabrication of very large scale integrated silicon circuits due to the relative ease, simplicity, and good controllability of the process. In this process, chemicals in the gas or vapor phase are reacted at the surface of the substrate where they form a solid product [10]. With CVD, it is possible to produce any metal and non-metallic element. This technology is now an essential factor in many optical and opto-electronic applications. The most important and widely used CVD processes are atmospheric pressure CVD (APCVD), low pressure CVD (LPCVD) and plasma enhanced CVD (PECVD) [10]. Low pressure chemical vapor deposition (LPCVD) was rapidly accepted due to its advantages.

2.1.1 The Advantages of LPCVD

Most low pressure CVD processes are conducted by resistance heating and less frequently infrared radiation heating techniques to attain isothermal conditions so that the substrate and the reactor walls are of similar temperature. The deposition rate and

uniformity of the films created by all CVD processes are governed by two basic parameters [11], [12]:

(I) The rate of mass transfer of reactant gases to the substrate surface

(II) The rate of surface reaction of the reactant gases at the substrate surface.

Lowering the pressure to below atmospheric pressure enhances the mass transfer rate relative to the surface reaction rate. Hence, the rate-determining step in the sequence is the surface reaction. Mass transfer rates depend mainly upon reactant concentration, diffusivity, and boundary layer thickness, which is related to reactor configuration, flow velocity, distances from edges, etc. Surface reaction rates depend mainly on reactant concentration and temperature. Therefore, in such a low pressure operation, much less attention need to be paid to the mass transfer variables that are so critical at atmospheric pressure [13].

Studies have shown capital, labor, power and gas cost per wafer to be nearly an order of magnitude below the standard atmospheric methods, let alone plasma CVD. The major reason for this cost breakthrough is the very high packing density available with stand-up closely packed wafer loading. The use of a low pressure results in a reactor condition such that mass transfer limitations at very close wafer spacing are unimportant compared to the rate of the chemical reaction at the wafer surface. With the surface reaction rate controlling the deposition, the uniform temperature inherent in a resistance-heated furnace leads to excellent uniformity of film thickness and composition [14].

2.1.2 LPCVD of Undoped and Doped Silicon Dioxide

Chemical Vapor Deposited silicon dioxide films, and their binary and ternary alloys find wide use in VLSI processing. These materials are used as insulation between polysilicon and metal layers in multilevel metal systems, as getters, as diffusion sources, as diffusion and implantation masks, as capping layers to prevent outdiffusion, and as final passivation layers. These materials are also widely used in optical industry [15].

There are various reactions that can be used to prepare undoped and doped CVD SiO_2. The reason for its promising applications lies in its versatility for depositing a very large materials at very low temperatures. The choice of the reaction is dependent on the temperature requirements of the system, as well as the equipment available for the process. The deposition variables that are important for undoped and doped CVD SiO_2 include temperature, pressure, reactant concentrations and their ratios, presence of dopant gases, system configuration, total gas flow, and wafer spacing [16].

In the past, undoped and doped silicon dioxide films have usually been deposited at atmospheric pressure by oxidizing silane with oxygen, nitrous oxide, or carbon dioxide at 300°-500°C [16], [17], [18]. Other chemical reactions for depositing silicon dioxide at atmospheric pressure have been investigated, but no major advantages have been observed. The overall reaction for the oxidation of silane and phosphorus by nitrous oxide are assumed to be [18], [19]

$$SiH_4 + 4N_2O \Longrightarrow SiO_2 + 2H_2O + 4N_2$$

$$2PH_3 + 8N_2O \Longrightarrow P_2O_5 + 3H_2O + 8N_2$$

For the SiH_4 and O_2 reaction, the overall reaction can be summarized as

$$SiH_4 + O_2 ===> SiO_2 + 2H_2$$

$$4PH_3 + 5O_2 ===> 2P_2O_5 + 6H_2$$

Later, due to the advantages of LPCVD, silicon dioxide films have been deposited at reduced pressure. Early low pressure work was reported by Sandor in 1962 [20], by Kern in 1965 [21], and by Oroshnik and Kraitchman in 1968 [22]. It involved the deposition of undoped SiO_2 at 730^0-750^0C from tetraethoxysilane (TEOS) in a hot-wall reactor. Kern deposited and characterized pyrolytic silicon oxide films prepared by LPCVD at temperatures as low as approximately 250^0C [21], [23].

Unfortunately, the advantages of LPCVD do not exist when phosphorus-doped silicon dioxide is deposited at reduced pressure using the reaction of silane, phosphine, and oxygen at 350^0-400^0C. The step coverage of films deposited at these low tempertures is nonconformal. Heat-treatment at ~1100^0C is usually used to flow the glass in order to get uniform step coverage. This high temperature treatment is not acceptable for very short channel devices where shallow junctions are required. Hence, there have been some reports of the deposition of PSG films in the mid-temperature range (600^0-800^0C) at reduced pressure, using the decomposition of organosilicon and organophosphorus compound. The results indicate an improved step coverage [24], [25].

LPCVD of binary and ternary silicate glass films was described by Kern in 1965 [21]. He used low pressure conditions (50 Torr at 730^0C) to achieve greatly improved uniformity of the films and to eliminate structural imperfections by preventing decomposition buildup on the reactor walls. The reactants used were TEOS, trimethyl borate, trimethyl phosphate, tetraethyl lead, and aluminum isopropoxide. Lead borosilicate glass films exhibitd particularly good passivation properties on silicon

devices. Tanikawa et al deposited doped SiO_2 films using n-propylsilicate, $Si(OC_3H_7)_4$ [24], as the Si source, and trimethyl phosphate and tripropyl borate as the doping cources. They showed the thickness uniformity as a function of pressures from 0.4 to 0.7 Torr and temperatures from 725^0 to 800^0C. They also indicated excellent uniformity of drive in from the doped films, and of the resulting concentration profiles in silicon substrates. However, contamination caused by particles of silicon dioxide particles falling from loose deposits on the reactor walls is a problem for both the processes.

2.2 Properties of Undoped and P-doped Silicon Dioxide Films

2.2.1 Undoped Silicon Dioxide Films

In general, the deposited oxide films must exhibit uniform thickness and composition, low particulate and chemical contamination, good adhesion to the substrate, low stress to prevent cracking, good integrity for high dielectric breakdown, conformal step coverage for multilayer systems, low pinhole density, and high throughput for manufacturing. Some of the properties obtained for thermal oxide are shown in table 2.1 [26].

CVD silicon dioxide is an amorphous structure of SiO_4 tetrahedra with an empirical formula SiO_2. Depending on deposition conditions, CVD silicon dioxide may have a lower density and slightly different stoichiometry from thermal silicon dioxide, causing changes in mechanical and electrical film properties (such as index of refraction, etch rate, stress, dielectric constant and high electric field breakdown strength). Deposition at higher temperatures, or use of a separate high temperature post-deposition anneal step can make the CVD films approach those of thermal oxide.

Table 2.1: Properties of Thermal Silicon Dioxide

Boiling Point(°C)	~2950
Melting Point (°C)	~1700
Molecular Weight	60.08
Refractive Index	1.46
Specific Heat (J/g°C)	1.0
Stress in film on Si (dyne/cm^3)	2-4 x 10^9, compressive
Thermal Conductivity(W/cm°C)	0.014
Dc Resistivity (Ω-cm), 25°C	10^{14}-10^{16}
Density (gm/cm^3)	2.27
Dielectric constant	3.8-3.9
Dielectric Strength (V/cm)	5-10x10^6
Energy Gap (eV)	~8
Etch rate in buffered HF (Å/min)	1000
Linear Expansion Coefficient (cm/cm°C)	5x10^{-7}

Deviation of the CVD silicon dioxide film's Properites, from that of the thermal SiO_2 value is often used as an indicator of film quality. For example, the refractive index of CVD SiO_2 greater than 1.46 indicates a silicon rich film, while smaller values indicate a low density, porous film. CVD SiO_2 is deposited with and without dopants, and each has unique properties and applications.

2.2.2 Phosphosilicate Glass

The addition of small amounts of phosphorus to silica films has several functions including changing the refractive index, lowering the melting point of silica glass and hence reducing the film reflow temperature, reduction of silicon film stress, modification of the thermal expansion coefficient, and densification of the silica-based film. Therefore, The properties of phosphorus doped silicon dioxide are considerably different from those of undoped CVD SiO_2. PSG is well known as an effective passivation material against Na^+ ions. Its dielectric constant and film stress are as low as that of SiO_2. PSG can be flowed at lower temperatures to create a smoother surface topography, and thereby facilitate the step coverage of subsequently deposited films. PSG becomes highly hygroscopic at higher phosphorus levels [15].

2.3 Phosphosilicate Glass

2.3.1 PSG Water Absorption and PSG Structure

PSG is a binary glass which consists of two compounds —P_2O_5 and SiO_2. It is expected that physical characteristics of the phosphorus doped silica glass are related to the chemical structure and composition of the phosphorus species in the silica network. However, since electron diffraction of the PSG film gives holo pattern in every case, sufficient knowledge in the film structure has not yet been obtained. A phase diagram of SiO_2-P_2O_5 system has been reported by Tien et al.[27], by saturated equilibration and quenching technique on bulk materials. Eldridge et al. [28] dealt with PSG film with gaseous P_2O_5 over a temperature range from 800^0 to 1200^0C. According to their results, small, water-soluble crystallites were formed on the surface of a film formed at 870^0C or

less, and from the SiO_2-P_2O_5 phase diagram of Tien et al., these small crystallites were assumed to be $2SiO_2 \cdot P_2O_5$ or $SiO_2 \cdot P_2O_5$. When the PSG films were formed at a relatively low temperature, phosphorus in the film can be considered to be in such a state that small particles of phosphorus oxide P_2O_5, rather than a compound such as $2SiO_2 \cdot P_2O_5$ or $SiO_2 \cdot P_2O_5$, are dispersed in the SiO_2 matrix [29]. At low phosphorus oxide concentration in the PSG film, the SiO_2 matrix which is water-insoluble protects the phosphorus oxide from being attacked by water. However, as the phosphorus oxide concentration increases to certain critical concentration, the volume fraction of phosphorus oxide to the SiO_2 matrix increases, and the SiO_2 matrix is no longer effective in protecting the phosphorus oxide from a moisture attack. The SiO_2 matrix has a larger angular distribution width of Si-O-Si bond when it is formed at low temperature [30]. Also, it is highly porous [31].This probably allows water to penetrate into the film with ease causing phosphorus oxide to dissolve. Heat-treatment densifies the SiO_2 matrix, which in turn makes it hard for water vapor to diffuse and attack the phosphorus oxide. It is likely that heat-treatment leads to reaction of the phosphorus oxide with the SiO_2 matrix, and results in formation of water-insoluble compound such as $(SiO_2)_x(P_2O_5)_y$.

2.3.2 Reflow of PSG

PSG can be flowed at lower temperatures to create a smoother surface topography, and thereby facilitate the step coverage of subsequently deposited films [32], [33]. The flow step is performed at 1000-1100°C, at pressures 1-25 atm, and in gas ambients of H_2O, N_2 and O_2. PSG becomes highly hygroscopic at higher phosphorus levels. Thus, it is recommended that the concentration in the oxide film be limited to 6-8 wt %P to

minimize phosphoric acid formation, and consequent Al corrosion. If the PSG is to be used a s a passivation layer, the maximum permitted phophorus content is 6%.

2.3.3 Phosphorus Concentration and its Measurement

Phosphorus oxide concentration is an important parameter of the PSG film. It is known empirically that, as the phosphorus oxide concentration increases, the film will absorb water more easily. The film properties, e.g., reflow temperature and thermal expansion, are controlled largely by fixing the phosphorus content of the films [34]. The phosphorus content, in the form of P_2O_5 in annealed PSG films, is typically held within a 2 to 8 w/o range. At 8 w/0 P and above, the films can become excessively hygroscopic, produce corrosive compounds, and form microcrystallites, while at 2 w/o P and below the P doping does not modify the film properties enough to be useful. So it is important to be able to control and determine this composition. Composition control is frequently achieved by controlling temperature and reactant gas composition during chemical vapor deposition of the PSG film.

Phosphorus content is an important factor in the fabrication of the wave guide used for the integrated device. A balance has to struck between having a high enough P content for the required refractive index and low enough lest it should become hygroscopic. Another important aspect to be kept in mind is that excess P (above 7.5%) would make the film absorbing which is undesirable.The properties of PSG which make it useful in a given application may depend on its composition. Hence, it must be possible to determine and control this composition [15], [34].

The concentration of phosphorus in silica glass can be measured by a dozen techniques, including direct chemical analysis, neutron activation analysis, infrared absorption, electron microprobe, etch rate variation, sheet resistivity after a standard diffusion and variation in the refractive index of the films, with a wide range of accuracy, sophistication, and effort, as summarized following [35].

2.3.3.1 Refractive Index Technique In the refractive index technique, previously the index of refraction has been determined by Raman spectroscopy. The refractive index of the samples is found at various positions on the wafer and the refractive index is averaged out. The P content of the given sample is found by comparing it with the calibration plot of refractive index *vs* P content [36], [37].

2.3.3.2 Etch Rate Technique In the etch rate variation technique, the samples are etched at 25°C using P-etch solution (2 parts 70% HNO_3, 3 parts 49% HF, 60 parts H_2O). The etch rates are determined by plotting film thickness *vs* the etch time. The etch rate calibration curve, i.e. a plot of etch rate Vs P content will give the P content for the given sample [38], [39].

2.3.3.3 Chemical Analysis : The films are dissolved in hydrofluoric acid, the sample size determined by weight loss, and the dissolved phosphorus converted to phosphate by addition of nitric acid. The phosphate is coprecipitated as beryllium phosphate and counted by x-ray fluorescence. The technique is calibrated using standard solution of known phosphate concentration [40].

2.3.3.4 Infrared Absorption Technique The composition of phosphosilicate glass can be analyzed by infrared absorption plot. The ratio of the intensity of the P=O absorbance band at ~1325 cm^{-1} to that of the Si-O band at ~1050 cm^{-1} can be correlated with the composition of vapor deposited phosphosilicate glasses over the range 0-20 mol per cent P_2O_5. Composition determinations based on the IR spectra of vapor deposited borosilicate and arsenosilicate glasses have proven useful. The IR reflectance spectra of silicate glasses have been employed as a qualitative test for the presence of phosphorus oxide. Tenney and Ghezzo have proposed a method to determine compositions of PSG. From the infrared plot, the linear absorption ratio for the glass (Fig.2.1)

$$R= (A-B)/(A'-B')$$

This ratio as a function of the glass composition for different temperatures was plotted by Tenney et al. Based on their results, a calibration curve was plotted for 700°C. A similar approximation for the P=O band area and a corresponding calibration curve was obtained. Employing the band area ratio

$$R^{*}=\{(A-B)x(C-D)\}/\{(A'-B')x(C'-D')\}$$

An average of both the methods was used to obtain the %phosphorus in the given glass.

In this work, we use FTIR to get the rough chemical composition of PSG according to the work of Tenney et al [41], [42], [43].

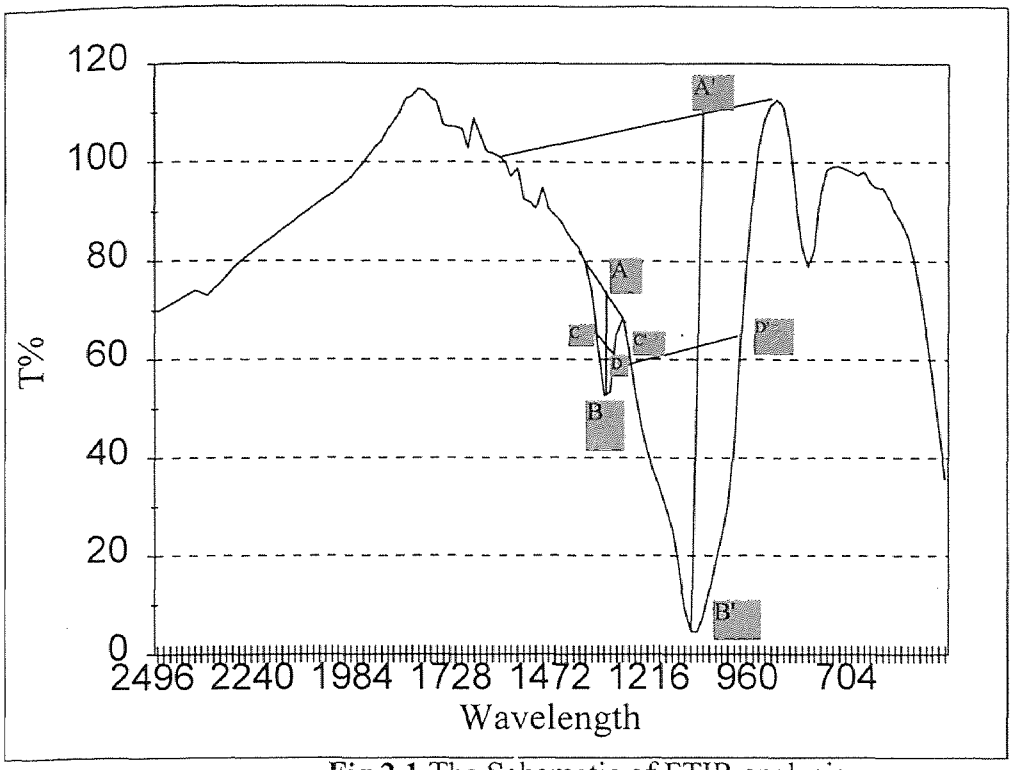

Fig.2.1 The Schematic of FTIR analysis

2.4 Previous Work for this Project

The synthesis and characterization of silicon dioxide films deposited on silicon wafers by LPCVD using ditertiarybutylsilane (DTBS) as a precursor and oxygen as the oxidant by former students. In their study, the dependence of film growth rate on various process parameters were studied and the results are reviewed here as a standing point of this work [44], [45].

These films were synthesized in the temperature range of 550 to 850 ^{0}C at a constant pressure of 0.2 torr, a DTBS flow rate of 10 sccm, and varied an O_2 flow rate to get desired flow rate of DTBS/O_2 ratio. The growth rate was found to follow an Arrhenius curve with the variation in the temperature with an activation energy of 12.6 kcal/mol. The growth rate was found to be proportional to the wafer space and inversely

proportional to the temperature in the range 550-750 ^{0}C. They found out that producing of crack-free thick oxide could be performed at 700 ^{0}C with flow rate ratio O_2/DTBS=10/1 with high growth rate.

In this work, the flow rate ratio of O_2/DTBS was kept at 15/1 based on the results of the previous study (10/1). The increasing of oxygen flow rate is due to the addition of TMP into the reaction of oxygen and DTBS. The effect of addition of Treimethylphosphite (TMP) was investigated, and finally the best combination of experimental parameters to deposit uniform PSG with high transparency, low stress and with high growth rate was suggested for sensor application.

CHAPTER 3

EXPERIMENTAL SETUP AND CHARACTERIZATION TECHNIQUES

3.1 Introduction

Silicon dioxide and phosphorus doped silicon dioxide thin films were synthesized in a LPCVD reactor altering various parameters like temperature, gas composition and time of deposition. The phosphorus oxide concentration in the PSG films is determined from the Fourier Transform Infrared analyses. Refractive Index and thickness of the films were measured by using ellipsometry and interferometry respectively. The optical transmission of the films was measured using a UV spectrophotometer. The literal transparency was also investigated by interferometer.

3.2 Deposition

3.2.1 Experimental Setup

3.2.1.1 The Substrates and Precursors

Substrate: Silicon dioxide and phosphosilicate glass films were deposited on (100) oriented single crystal, single-side polished Si wafers (obtained from Silicon Sense Inc.), and fused quartz wafers (obtained from Hoya, Japan). The details of the Si wafer are in table 3.1.

Table 3.1 Specifications of the Si wafer

Source	Silicon Sense Inc.
Diameter	100mm
Orientation	<100>
Thickness	525±25μm
Type/Dopant	p/Boron
Resistivity	5-15 Ω-cm
Grade	Test

Precursors: In this work, Silicon dioxide was deposited using an organic precursor, ditertiarybutylsilane (DTBS), and oxygen. DTBS has a chemical formula of $(C_4H_9)_2SiH_2$ and is a safe alternate precursor to SiH_4 with a flash point of 15°C. It is a colorless liquid with a boiling point of 128°C, vapor pressure of 20.5 torr at 20°C, and is commercially available from Olin Hunt as CONSi-4000 with a 99%+ chemical purity. Using DTBS as a precursor provided better results in terms of stress, uniformity, optical transmission and refractive index for the film to be used in the fabrication of Mach Zehnder interferometer. This work addresses the use of this organosilane precursor for synthesizing amorphous silicon dioxide films. The silicon dioxide thus deposited forms the cladding for the optic fiber. phosphorus dopant was added during the deposition in the form of trimethyl phosphite(TMP), to form a phosphosilicate glass (PSG). TMP is a colorless liquid with a chemical formula$(CH_3O)_3P$ with a molecular weight of 124.08 and melting point of

78°C. Trimethylphosphite can be added into the reaction chamber to obtain the required amount of phosphorus in the phosphosilicate glass.

3.2.1.2 LPCVD Reactor: The schematic for hot wall low pressure chemical vapor deposition reactor is shown in Fig 3.1. The reactor consists of fused quartz tube of 5 inches in diameter and about 50 inches in length. The tube is kept inside a Lindbergh three zone surface. The zone temperatures are controlled by manual settings. A maximum temperature of 1200°C can be reached using this furnace and a gradient of temperature can also be obtained inside the quartz tube. Heating is provided by Lindbergh silicon carbide heating elements. It is equipped with Plantinel II thermocouples which sense the temperature of the zone and the voltage developed which is used for automatic temperature control. The tube and the coils are surrounded with a ceramic enclosure. The tube is sealed on both the ends by end caps and metallic rings. During the heating process, thermal expansion of the O-rings may cause leakage in the system. To avoid this problem, water cooling is arranged by cold water circulation. Apart from this, additional cooling is provided by fans.

A MKS baratron gauge with a range of 10 Torr is used to monitor the pressure at the input end. The monitored pressure is displayed by the MKS display unit. A Mass Flow Controller (Type 252A Exhaust Valve Controller, by MKS Instruments, Inc.) is used to provide automatically control of pressure during specific deposition by connectting it to the outlet valve.

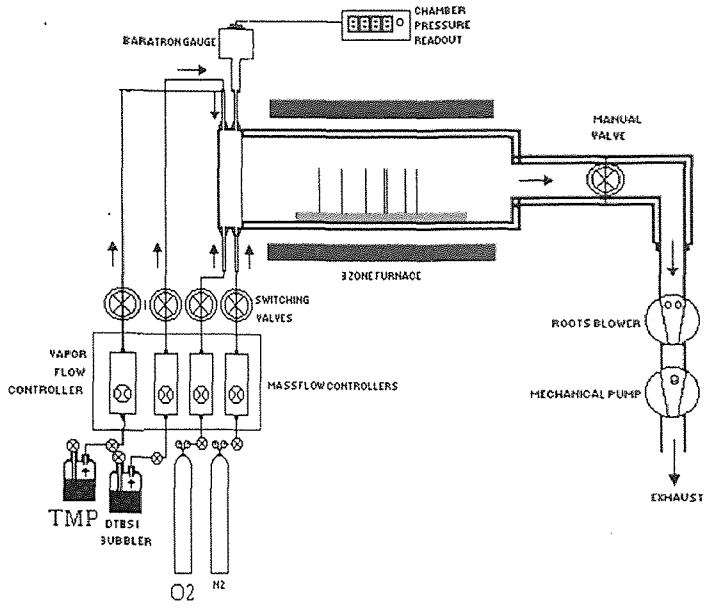

Figure 3.1 : A schematic of the LPCVD reactor

The system is kept at low pressure by vacuum pumps. This system uses a booster pump and a mechanical backing pump. The Booster pump is used to enhance the flow of gases and thereby the pumping speed. Mechanical backup does the real pumping and the combination provides a vacuum as low as a milliTorr. The Booster pump is a *Ruvac* single stage roots pump and the backing pump is a *Trivac* dual stage rotary vane pump. Nitrogen ballast gas is used in the pump to dilute any hazardous outgoing gas. An oil filtration system is also used to separate the micron size dust particles that are accumulated during the pumping process.

Wafers are loaded inside the tube using a quartz carrier boat. Wafers are kept vertically in the slots provided in the boat. The boat is kept inside the quartz tube and the tube is sealed by the inlet lid. A manual control valve is provided at the output end to control the rate at which the gas is removed from the reactor. The input seal consists of

three provisions for gas inlet, so that if more than one precursor is used, they will mix together and diffuse inside. In this experiment, the flow rate of DTBS is controlled by Type 550 Mass flow Control System which offers temperature control too. The flow rate of oxygen and TMP are also controlled by this kind of MFC but the readouts are offered by 4-channel Readout. Precursor is allowed through a pneumatic control valve provided at the input end. Unloading of the wafers is done by bringing the reactor to atmospheric pressure. This is done by closing the valve and passing a controlled flow of nitrogen into the chamber.

3.2.1.3 Leakage Check: A leak would result in a change in the deposit structure (due to oxygen) and could result in haze depending on the extent of the leak, therefore a leakage check in CVD is an important step before making an experiment. When carrying out leak check, all pneumatic controllers and gas regulators should be fully open to the gas cylinder main valves. The capillary is disconnected and the inlet is sealed with a plug because it is not possible to create vacuum in the capillary in the limited time period. After pumping the reaction system for a whole day, closing the outlet valve of the chamber, the pressure increasing rate was measured at a fixed period of time in the chamber to obtain the leakage rate. For this LPCVD system, the leakage rate deviated from 0.13 to 2 mTorr/min. Depending on the chamber condition a very low leak rate for a new chamber and higher leak rate for a chamber after long time in service should be seen. However, the leakage rate in this system was basically good.

3.2.1.4 Flow Rate Calibration: CVD reactors and other process systems require that the rates of introduction of the process gases into the process chambers be controlled. In some applications, this is achieved by adjusting the gas influx to maintain a constant chamber pressure. More commonly, the process gas flow is directly controlled. To do this, mass flow controllers are used. Mass flow controllers consist of a mass-flowmeter, a controller, and a valve. They are located between the gas source and the chamber, where they can monitor and dispense the gases at predetermined rates. The mass flow control system operates by controlling the differential pressure across a known conductance, calibrated flow element in order to provide closed-loop differential pressure control across that element. The mass flow rate of the desired vapor is simply conductance of the flow element times differential pressure in appropriate engineering units.

Gas flows were controlled by MKS type 550A Mass Flow Control System automatically. The pressure in the reactor was measured with a barratry gauge from MKS. The gas or vapor flow rate calibration was checked by delivering a fixed volume of gas (product of the metered flow rate and time) into the known reaction chamber volume. The pressure increase was measured and used to calculate the volume of the gas corrected to the standard condition. (0°C, 1 atm). According to the gas law, the flow rate corrected to STP (sccm) is given by the formula below:

$$\text{Flow Rate} = 60(\Delta P/\Delta t)(T_0 V/P_o T)$$

where ΔP = pressure increase in Torr,

$T_0 = 273$ K

P_0 = 760 Torr

V = volume of the chamber, cm^3

Δt = time of delivering gas, sec.

Routine flow rate calibrations were conducted before every run.

3.2.2 Deposition Procedure

The wafers were labeled and accurately weighed (up to 4 decimal places) using an electronic balance. These wafers were then placed on a quartz carrier boat with a dummu wafer on the its back side and loaded inside the tube. The wafers were placed at 3 cm distance from each other[45]. From front to rear downstreamly, the wafers were labeled as wafer1, wafer2, wafer3, which in the chapter 4 means the corresponding wafer positions. The boat was placed at a distance of 64 cm from the door.

After loading, the furnace was brought to low pressure by pumping down the chamber. The temperature was raised to the required level slowly in steps of about 250°C. The temperature was allowed to reach the set value in all the three zones before raising it further until the desired value is reached.

Once the required temperature was reached, the valves for oxygen flow were opened. When the flowmeter showed stabilized value of flow, the DTBS and TMP tanks were opened. The pressure was then set to the required value. Care was taken not to let the organic precursors into the chamber before there was oxygen flow lest the films should have carbon in them. Then the Oil filter was switched on.

3.3 Characterization of Phosphosilicate Glass Films

3.3.1 Thickness

Film thickness was measured by Nanospec interferometer which bases its estimation on the monochromatic light interface fringes formed within a zone limited by sample surface and a semi-transparent mirror. The device consists of Nanometrics Nanospec/AFT microarea gauge and SDP-2000T film thickness computer.

The thickness of the film deposited on the wafer was measured at five different points. Thickness Variations across a wafer are determined by measuring the film thickness at the center and ~10 mm from the edges of the wafer, and are given by the percentage difference between the thickest and thinnest points. The deposition rate was determined as the film thickness over the deposition time, and averaged over all the wafers in the run.

3.3.2 Refractive Index

The refractive index was determined by a Rudolph Research Auto EL ellipsometer, which consists of a polarizer and a compensator. Plane (45°) polarized light the polarizer is elliptically polarized when it passes through the compensator. It is then reflected by the sample surface, collected by a detector, analyzed for its intensity, and finally quantified by a set of delta psi values, which corresponds to the phase difference of the light reflected from the film surface and the interface [10]. The values were then fed to a computer which numerically solves an equation to give the refractive index of the film.

The refractive index of the film deposited on the wafer was measured at five different points and then averaged out to the refractive index of the wafer.

3.3.3 Infrared Spectra

The levels of interstitial oxygen and phosphorus were determined by using infrared absorption spectroscopy. The analysis was done on a Perkin-Elmer 1600 series FTIR spectrophotmeter to determine the characteristics of the deposits. A spectrum of percent transmittance or absorption was obtained for samples of known thicknesses.

The composition of phospho silicate glass can be analysed by infrared absorption plot. The ratio of the intensity of the P=O absorbance band at ~1325 cm^{-1} to that of the Si-O band at ~1050 cm^{-1} can be correlated with the composition of vapor deposited phospho silicate glasses over the range 0-20 mol per cent P_2O_5.

The properties of PSG which make it useful in a given application may depend on its composition. Hence, it must be possible to determine and control this composition. Composition control is usually achieved by controlling the temperature and reactant gas composition during the CVD of the PSG film. Composition determinations based on the IR spectra of vapor deposited borosilicate and arsenosilicate glasses have proven useful. The IR reflectance spectra of silicate glasses have been employed as a qualitative test for the presence of phosphorus oxide. Tenney and Ghezzo[41] have proposed a method to determine compositions of PSG. From the infrared plot, the linear absorption ratio for the glass (ratio of the linear absorption of PSG to that of pure SiO_2) is calculated. This

ratio as a function of the glass composition for different temperatures was plotted by Tenney et al [41]. Based on their results, a calibration curve was plotted for 700°C.

A similar approximation for the P=O band area and a corresponding calibration curve was obtained. An average of both the methods was used to obtain the phosphorus content in the given glass.

3.3.4 Stress

The stress in the film was determined by a house developed device, employing a laser beam equipment which measures change in radius of curvature of the wafer resulting from the film deposited on one side. Two fixed and parallel He-Ne laser beams were incident on the wafer surface before and after deposition. The reflected beams from the two surfaces was then projected by an angled plane mirror as two points onto a scale in a certain distance, and thus, their separation can be measured more accurately. The change in separation of these two points was fed into Stony's Equation to obtain actual stress value. The calculation formula is:

$$\delta = 12.3\ D/T$$

where D = distance difference between two points after and before deposition (mm);

T = thickness of the films, (λm);

δ = stress of the film (MPa), negative value indicates tensile stress

3.3.5 Optical Transmission

If there was carbon in the film, the transmission of the films would degrade. The effect of carbon to the film transmission is detectable by UV light. So the optical transmission for

the phosphosilicate glass was measured from the films deposited on quartz wafers by using a UV-spectrophotometer. The transparency was also checked by using interferometer to let light pass the films laterally.

CHAPTER 4

RESULTS AND DISCUSSION

4.1 Introduction

The results of phosphosilicate glass thin films synthesized on Si and quartz substrates at a constant pressure of 0.2 Torr, at different temperatures between 600°C and 700°C, and at various flow rates of TMP are presented in this chapter.

4.2 Deposition of PSG

4.2.1 The Effect of Wafer to Wafer Space

In LPCVD, the wafer to wafer space has an extremely critical effect on deposition rate. It was observed that, in the PSG deposition, the deposition rate increased by a fact of 2 if the wafer to wafer space was increased by a fact of 8 within certain range. This shows that the mass transfer rate was increased by increasing the wafer spacing. However, the uniformity of the PSG films was getting worse by increasing the wafer to wafer space.

4.2.2 The Effect of TMP Flow Rate and Temperature on Deposition Rate

The results show that the silicon dioxide deposition rate is strongly enhanced in the presence of TMP. The dependence of the deposition rate on TMP flow rate is presented in Fig.4.1. The deposition rate increases with increasing TMP flow rate, tends to saturate at the TMP flow rate of 5 sccm, reaches a maximum, and decreases at high TMP flow rates.

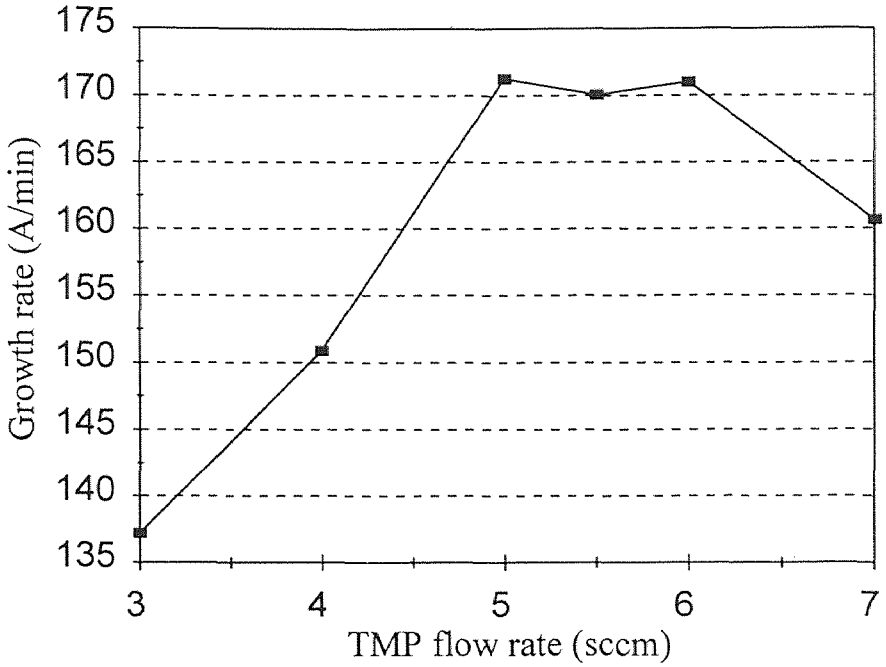

Fig.4.1 PSG growth rate vs TMP flow rate, DTBS/oxygen=1:15

The temperature dependence of the deposition with TMP added is shown in Fig.4.2. An Arrhenius behavior could not be observed; there is a maximum of growth rate at 650 ^{0}C. The deposition rate always increases when phosphorus oxide source is present, indicates that TMP catalyzes the deposition.

Enhancement in the silicon dioxide deposition rate in the presence of a phosphorus oxide source has been observed previously in other low pressure depositions where inorganic as well as organic sources for SiO_2 and P_2O_5 were used [25], [46]. The

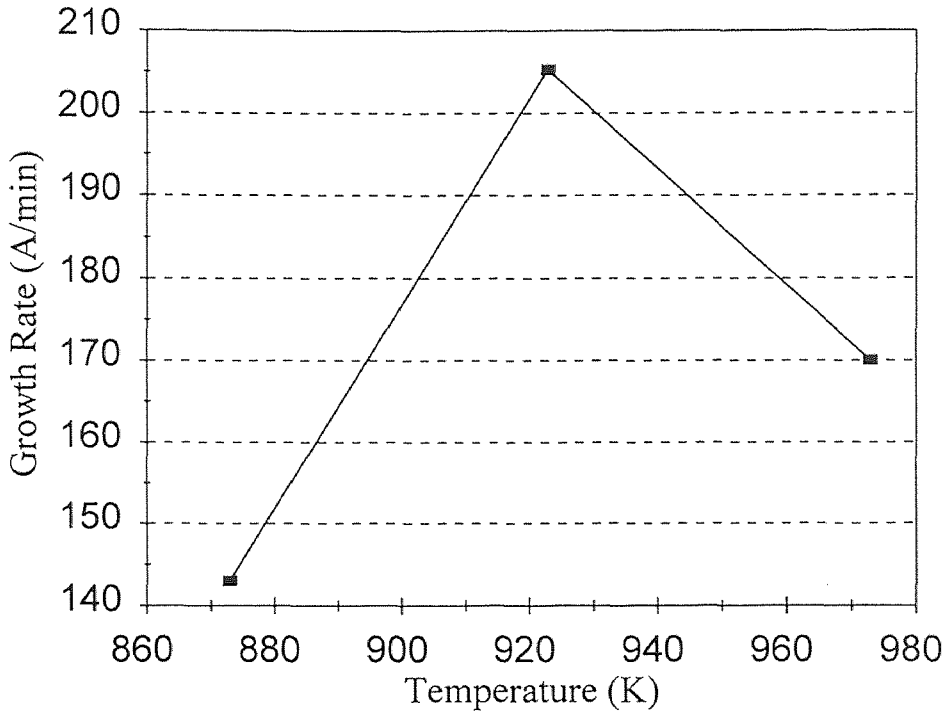

Fig.4.2 The effect of temperature on growth rate of PSG
DTBS:Oxygen:TMP=2:30:1

increase-maximum-decrease behavior of the deposition rate obtained with increasing TMP flow rates can be explained by the retardation theory [19]. Atmospheric pressure CVD experiments indicate that oxygen behaves as a retardant in the oxygen-hydride reaction, as a result a maximum appears in the deposition rate with increasing oxygen flow rate. The maximum tends to shift toward higher oxygen flow rate and to broaden with increasing hydride flow rate or increasing temperature [47].

Depletion in the deposition rate usually exists in the deposition of PSG. The depletion in the deposition rate is defined as:

$$\frac{\text{Dep. Rate (wafer1) - Dep.Rate (wafer2 or 3)}}{\text{Dep. Rate (wafer1)}} \times 100$$

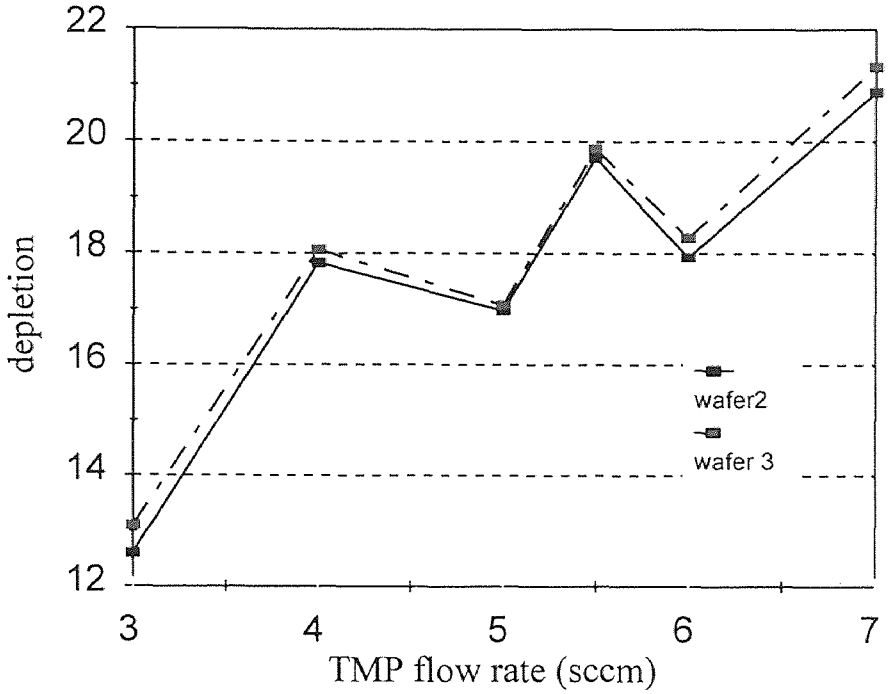

Fig.4.3 Depletion vs TMP flow rate, DTBS/oxygen=1:15

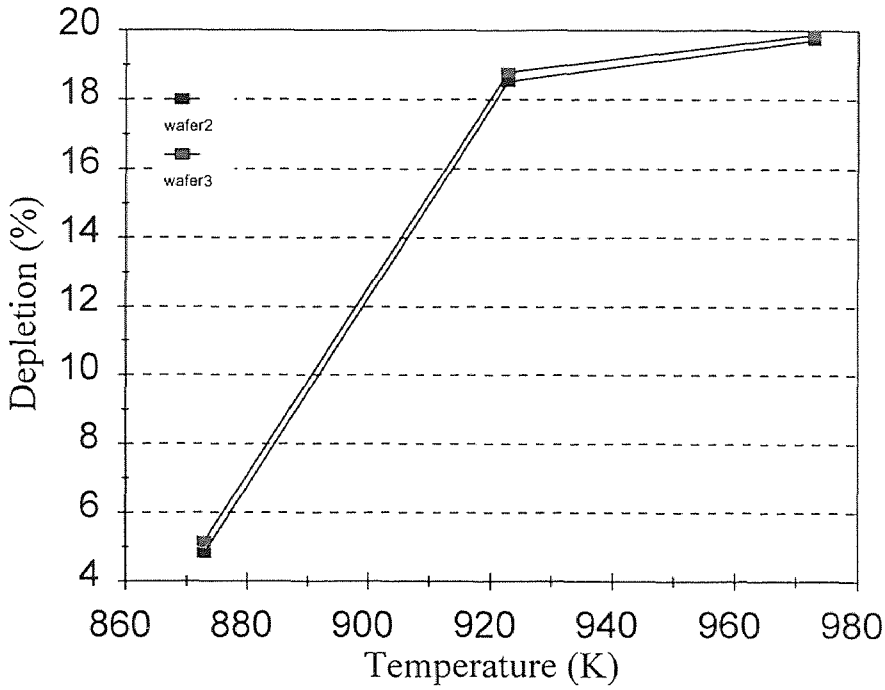

Fig.4.4 The depletion of PSG vs temperature
DTBS:Oxygen:TMP=2:30:1

The results are summarized in Fig.4.3 and Fig.4.4 where the depletion is given as a function of the TMP flow rate and temperature respectively. It was found that the depletion increases with increasing TMP flow rate and temperature. This phenomenon corresponds to the consumption of reactant gas. Thus the partial pressure of the gases in the deposition zone is reduced and the deposition at the rear is slower than that at the front. However, as shown in Fig.4.4, the decreasing of deposition temperature decreases the depletion rapidly.

4.2.3 The Effect of TMP Flow Rate and Temperature on Uniformity

The changes in the thickness uniformity in terms of thickness variation with the deposition conditions is presented in Fig.4.5 and Fig.4.6. The variation in the film thickness increases with increasing TMP flow rate. Decreasing the temperature causes an improvement in the thickness uniformity across the wafer.

A FTIR results in Fig.4.7 shows the composition uniformity across the wafer. We could not found the composition variation across the wafer by FTIR. Fig.4.7 shows that the composition uniformity is quite good.

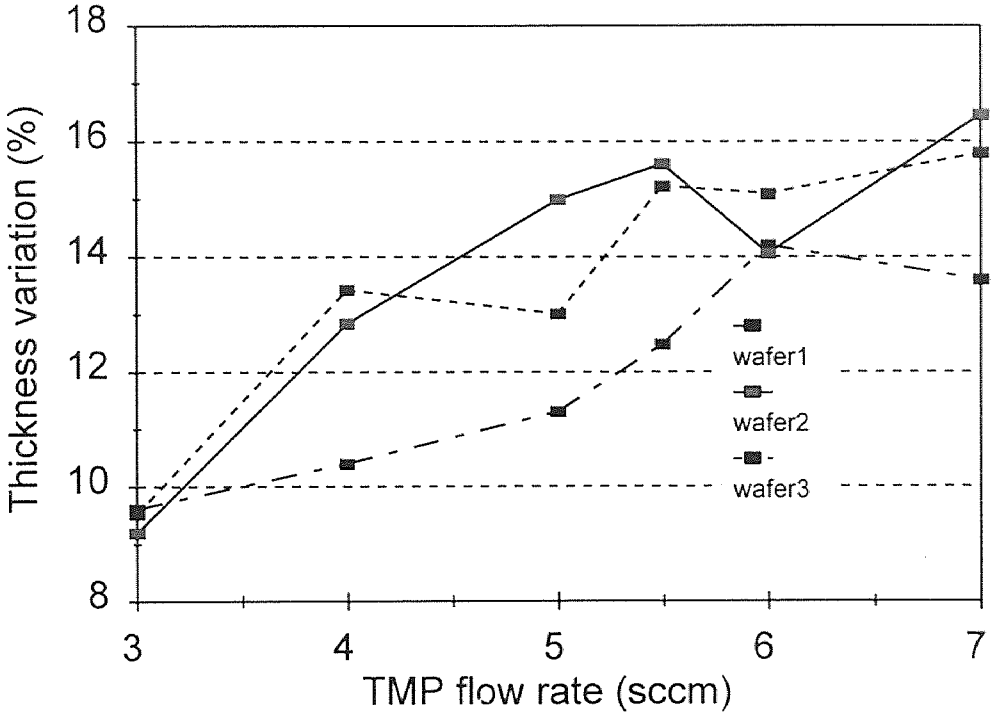

Fig.4.5 Thickness variation vs TMP flow rate, DTBS/oxygen=1:15

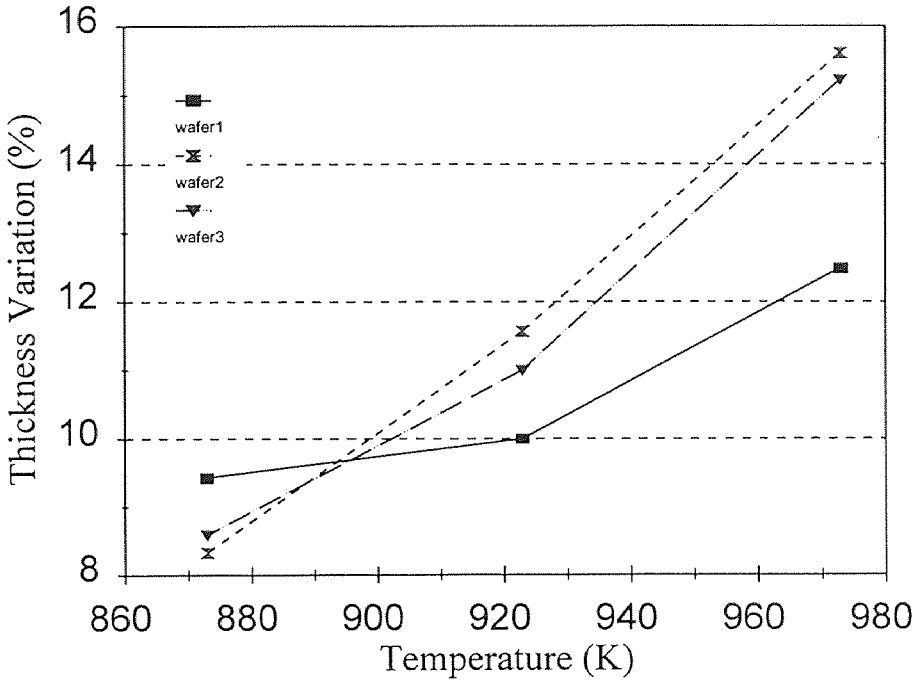

Fig.4.6 Thickness Variation vs Temperature
DTBS:Oxygen:TMP=2:30:1

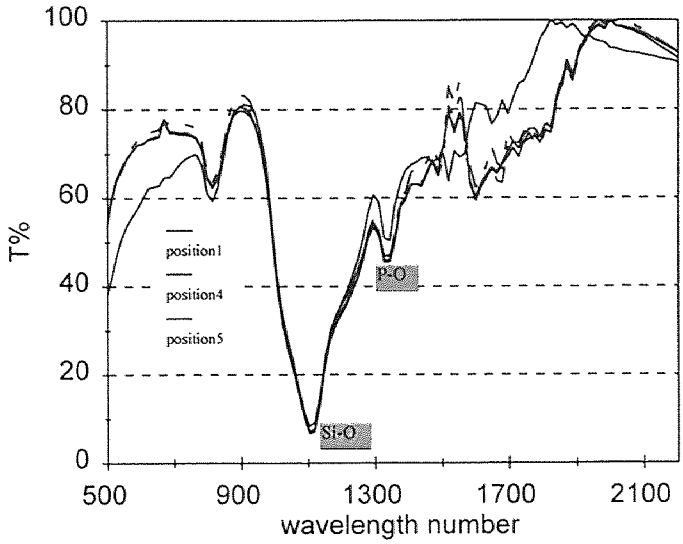

Fig.4.7 FTIR results at different position across the same wafer
Flow rate ratio is DTBS:oxygen:TMP=10:150:7

4.2.4 The Effect of TMP Flow Rate and Temperature on Phosphorus Oxide Concentration

The phosphorus oxide concentration increases with increasing TMP, and tends to saturate at high TMP flow rate (Fig. 4.8). It decreases when the temperature is increased (Fig.4.9), however, we found that there is a maximum at the 650 ^{0}C. This may indicate that the reaction between TMP and oxygen could be enhanced by decreasing the temperature.

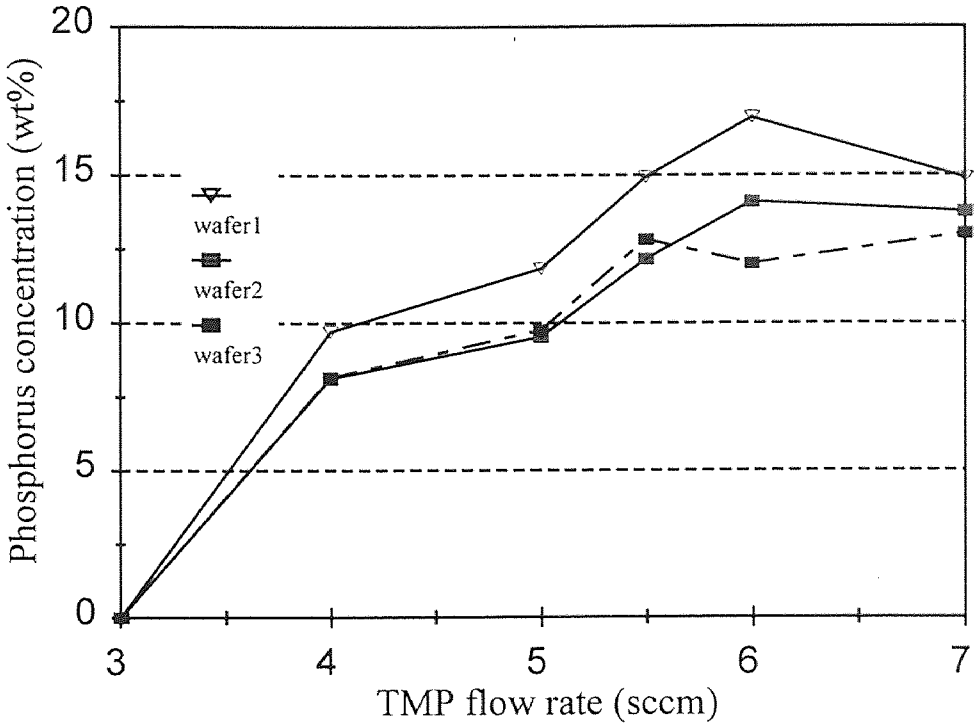

Fig.4.8 The effect of TMP flow rate on phosphorus oxide concentration
DTBS/oxygen=1:15

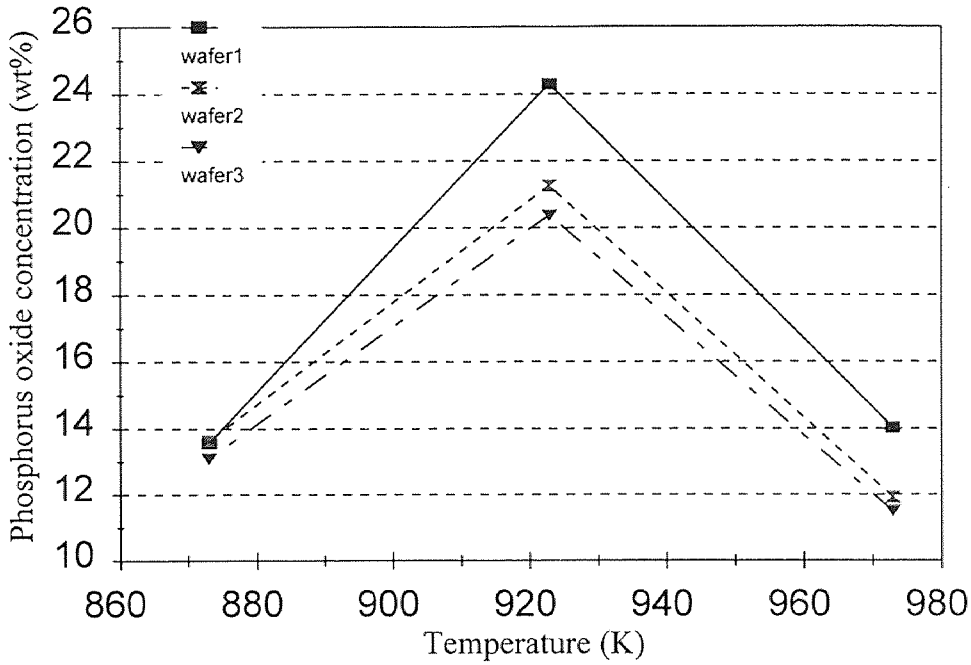

Fig.4.9 The effect of deposition temperature on P content
DTBS:oxygen:TMP=2:30:1

As the aforementioned, the addition of TMP to the reaction of DBTS and oxygen increase the deposition rate, decreases the apparent activation energy, and causes the thickness uniformity to degrade. However, the thickness uniformity can be enhanced slightly by increasing temperature. In the other hand, the phosphorus oxide concentration is decreased by the increasing the temperature. Hence, a comprise should be made to obtain the best combination of deposition parameters.

4.3 Physicochemical Properties of PSG Films

4.3.1 Density of PSG Films

Fig.4.10 shows the effect of TMP flow rate on density of PSG films. It shows the same increase-maximum-decrease behavior as the effect of TMP flow rate on deposition rate. When the TMP flow rate is not too high, the phosphorus oxide added densified the films. The corresponding concentration showed in Fig.4.8 may give the explanation for this result.

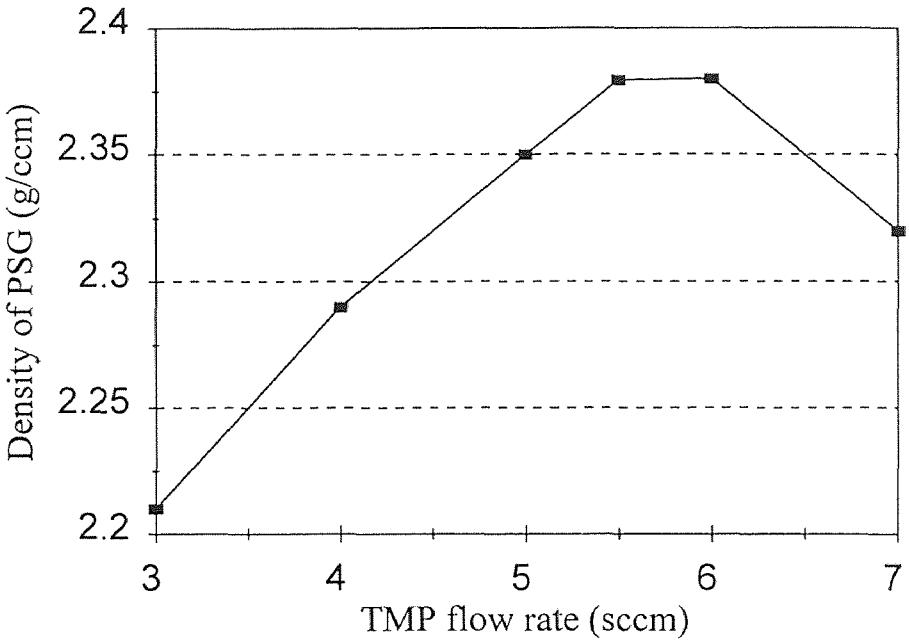

Fig.4.10 The density of PSG vs TMP flow rate, DTBS/oxygen=1:15

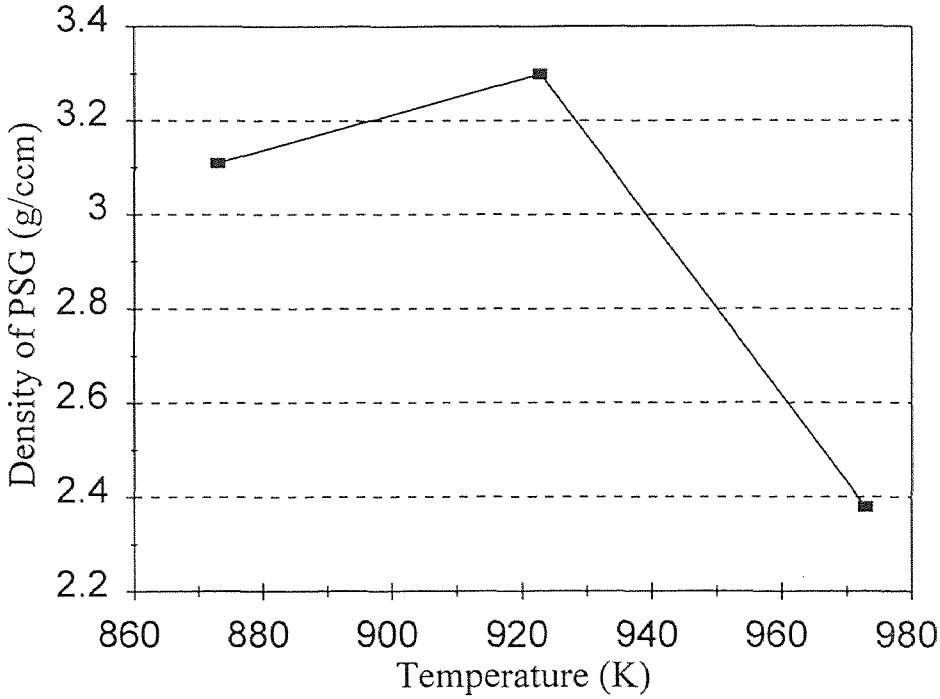

Fig.4.11 The effect of deposition temperature on density
DTBS:Oxygen:TMP=2:30:1

Fig.4.11 shows that the density of PSG films vs temperature, the density is very high when it was deposited at 650 ^{0}C, that may be explained that the phosphorus oxide concentration is higher when the PSG film was deposited at this temperature.

4.3.2 Stress of PSG Films

The stress in PSG films prepared in the current work is shown graphically in Fig.4.12 and Fig.4.13. The tensile stress in PSG films drops off gradually with increasing phosphorus content up to certain concentration and then increases as compressive stress. So the phosphorus oxide in silicon dioxide films can increase the stress compressively. This may be explained by the difference of the thermal expansion coefficient of the phases.

Fig.4.13 shows the stress vs deposition temperature. We can see that the stress decreases slightly when decreasing the temperature.

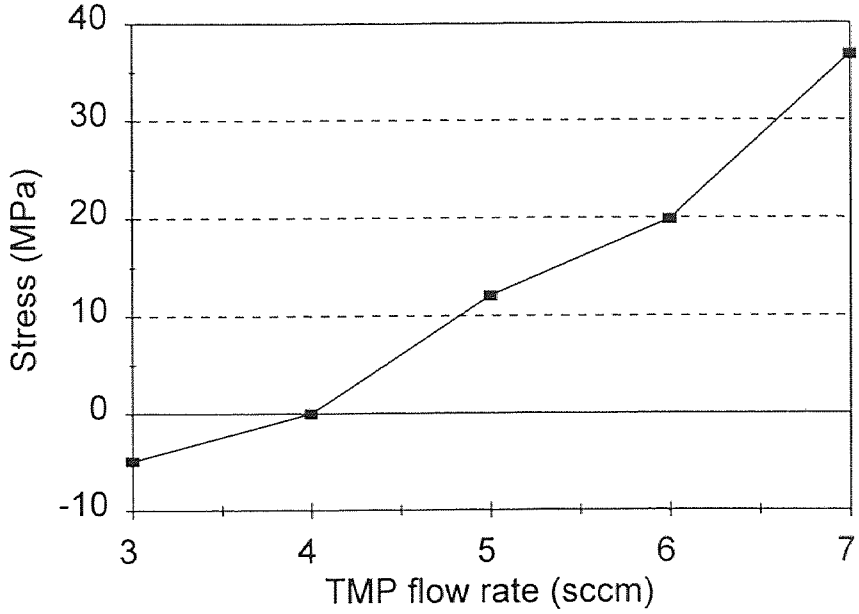

Fig.4.12 Stress of PSG films vs TMP flow rate, DTBS/oxygen=1:15

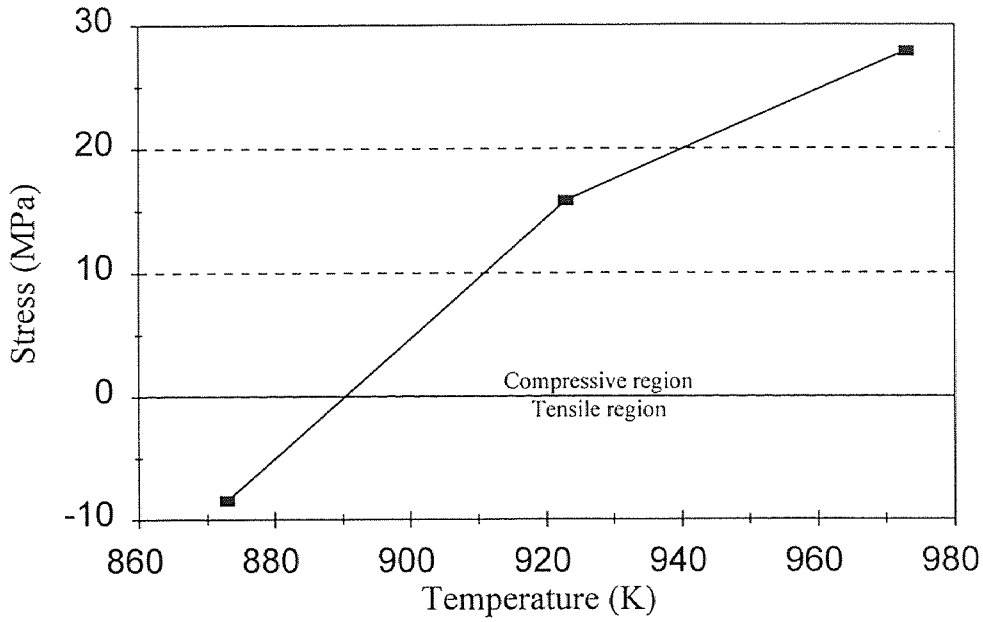

Fig.4.13 Stress of PSG films at different deposition temperature, DTBS:O_2:TMP=2:30:1

4.3.3 Refractive Index of PSG Films

The refractive index n of a film depends on its density and stiochiometry [48]. It grows on increasing the number of oxygen vacancies in oxide transparent films [49]. The refractive index of PSG films deposited at different TMP flow rate and temperature are shown in Fig.4.14 and Fig. 4.15. The refractive index was obtained by measuring 5 points in every wafer, the result is the average of the 5 points. As shown in Fig.4.14, the refractive index is quite high when the TMP flow rate is low and is different form wafer to wafer. This may be explained that when the TMP flow rate is low —that is the phosphorus oxide concentration is low, the distribution of phosphorus oxide is not uniform, thus we get some abnormal readout for refractive index, and hence higher refractive index for the film. As the TMP flow rate increasing, the phosphorus oxide concentration increases and then the distribution is becoming uniform, the result of refractive index obtained is consistent with the results of other works. When the TMP flow rate is around 5-6 sccm, the refractive index of the films is very uniform from wafer to wafer. However, the uniformity of the refractive index wafer to wafer degrades when the TMP flow rate increases. This is due to the increasing depletion when the TMP flow rate increases.

Fig.4.15 shows that the refractive index of the PSG films increases with the decreasing of the deposition temperature. This is consistent with other works. The increase in refractive index can be explained as due to the higher phosphorus oxide concentration and densification in the films. The uniformity on refractive index from

wafer to wafer degrade when decrease the deposition temperature. At 700 ^{0}C, the refractive index from wafer to wafer is quite the same.

4.3.4 Optical Transparency of PSG Films

The optical transmission for the PSG films was measured by UV spectrophotometer. The result shows that the transparency is quite the same with different TMP flow rate —different phosphorus oxide concentration (Fig.4.16). However, the transmission of the films increases with decreasing the deposition temperature (Fig.4.17). The ECSA analysis shows that there is carbon in the films deposited at 700 ^{0}C, but no carbon was found in the film deposited at 650 ^{0}C. We can also know the existence of carbon in the film by FTIR (Fig.4.18). The lower transmission of the films deposited at 700 ^{0}C due to the carbon in the films. The reaction which produces the carbon is controlled by decreasing the temperature.

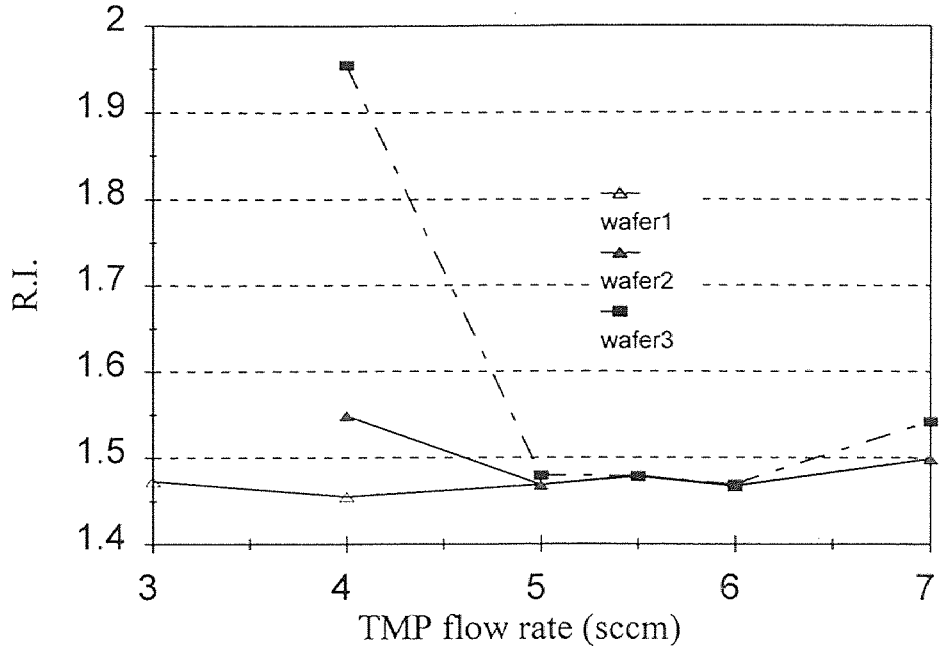

Fig 4.14 Refractive index vs TMP flow rate, DTBS/oxygen=1:15

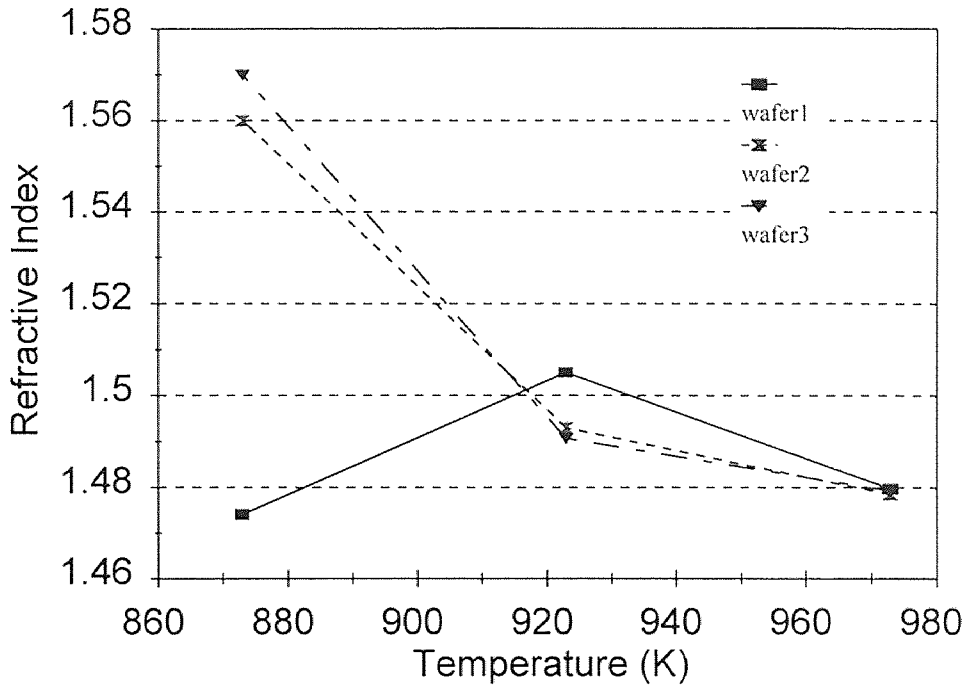

Fig.4.15 The effect of deposition temperature on Refractive Index of PSG, DTBS:O_2:TMP=2:30:1

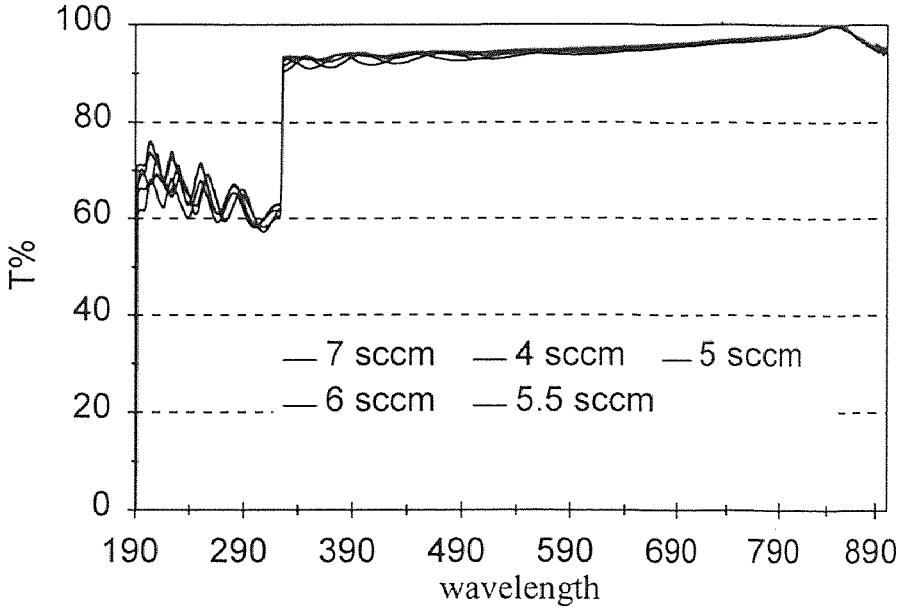

Fig.4.16 Transmission of PSG deposited at different TMP flow rate DTBS/Oxygen=1:15, Deposition temperature: 700 ^{0}C

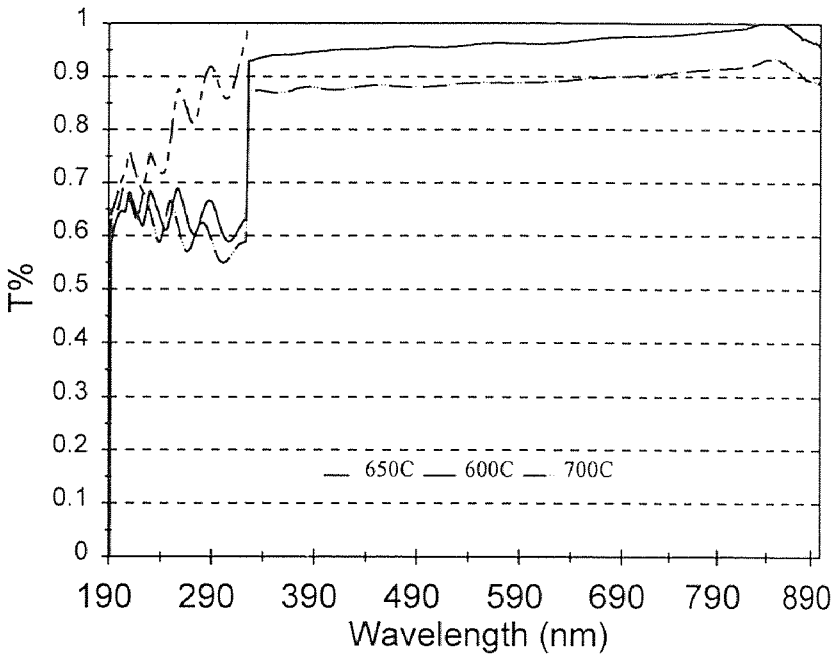

Fig. 4.17 Transmission of PSG deposited at different temperature, DTBS:O_2:TMP=2:30:1

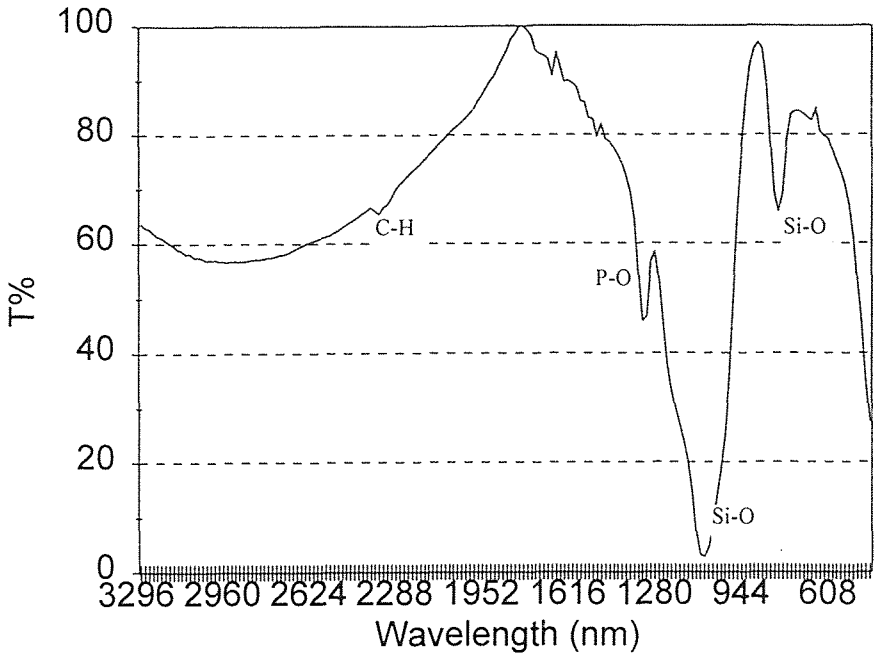
100
80
60
40
20
0
T%
C-H
P-O
Si-O
Si-O
3296 2960 2624 2288 1952 1616 1280 944 608
Wavelength (nm)

(a)

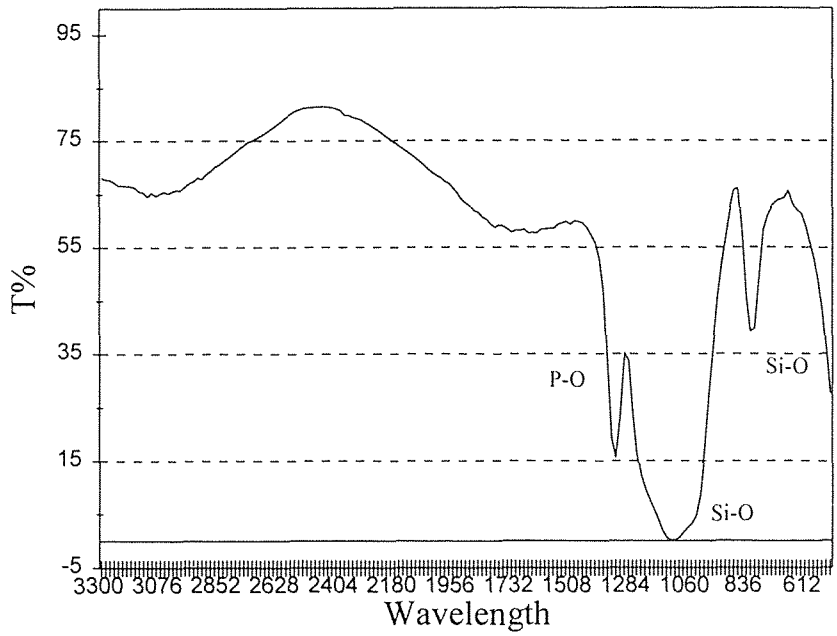
95
75
55
35
15
-5
T%
P-O
Si-O
Si-O
3300 3076 2852 2628 2404 2180 1956 1732 1508 1284 1060 836 612
Wavelength

(b)

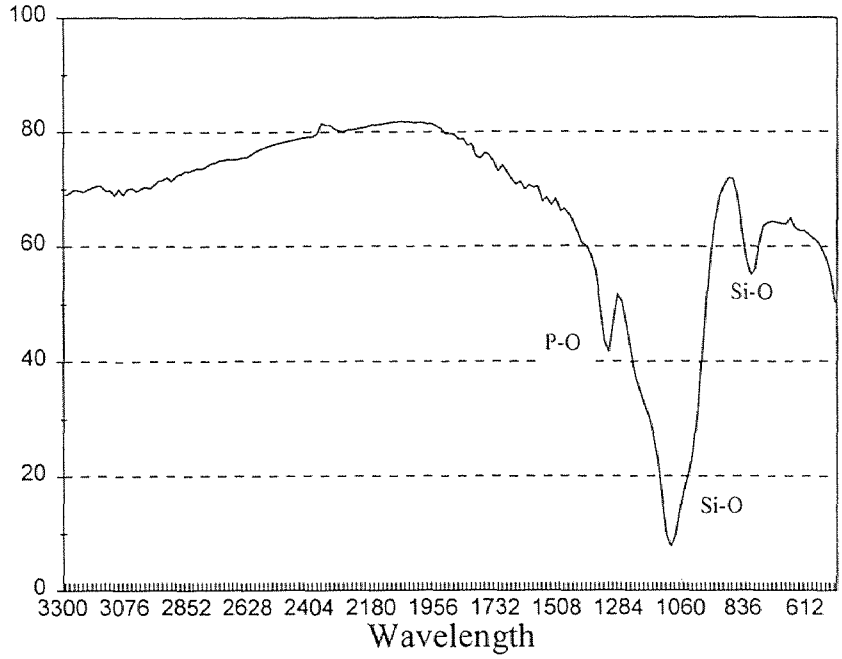

(c)

Fig.4.18 FTIR results at different temperature
(a) 700 ^{0}C, (b) 650 ^{0}C, (c) 600 ^{0}C

CHAPTER 5

CONCLUSIONS

Phosphosilicate glass thin films were synthesized on silicon and quartz wafers using Ditertiarybutylsilane(DTBS), Trimethylphosphite(TMP) and oxygen as precursors. The films were processed at different temperatures between 600°C and 700°C at a constant pressure, and at different flow rate of TMP.

The effect of TMP flow rate and deposition temperature on deposition parameters and the properties of PSG films were investigated. The films deposited were uniform, amorphous and the composition of the films varied with deposition temperature and TMP flow rate. The deposition rate increased with increasing TMP flow rate and had a maximum of deposition rate at 650 ^{0}C. It was suggested that the addition of TMP catalyzes the deposition. There was a maximum of density with increasing the TMP flow rate and deposition temperature. The stresses were very low tensile in the case of very low phosphorus oxide concentration, tended towards being less tensile, became compressive and tended towards increasingly compressive with increasing deposition temperature and TMP flow rate. Refractive index increased with increasing deposition temperature. A less transparent film at higher temperatures also suggested presence of carbon at higher temperatures, This may be due to a possible decomposition reaction. The PSG films showed around 100% transparency when deposited at 650 ^{0}C.

In summary, the best deposition parameters for PSG using DTBS, TMP and oxygen should be that the flow rate ratio of DTBS and oxygen is 1/15, and the deposition temperature is 650 ^{0}C while keep the pressure at 0.2 torr.

REFERENCES

1. J. W. Sadowski, "Review of Optical Methods in Immunosensing", *SPIE,* Vol.954, *Optical Testing and Metrology II,* 1988.

2. M. T. Hanagan, A. N. Sloper, and R. H. Ashworth, "From Electronic to Opto-Electronic Biosensors: An Engineering Review", *Anal. Chem. Act.*, Vol.213, p23-33, 1988

3. W. Lukosz, D. Clere, Ph. M. Nellen, Ch. Stamm, and P. Weiss, "Output Grating Coupling on Optical Waveguides as Direct Immunosensors", *Biosensors & Bioelectronics,* Vol.6, p227-232, 1991.

4. J. S. Schultz, "Biosensors", *Scientific Amer.*, p64-69, August, 1991.

5. S. Valette, S. Renard, J. P. Jadot, "Silicon-based Integrated Optics Technology for Optical Sensor Appliications", *Sensors and Actuators*, Vol. A21-A23, p987-1091, 1990.

6. N. Hartman, "Optical Sensors Detect Toxic Chemicals", *R&D Megazine,* Vol.13-14, March, 1990.

7. W. Kukosz and C. H. Stamm, "Integrated Optical Interferometer as Relative Humidity Sensor and Differential Refractometer", *Sensors and Actuators,* Vol.A25-A27, p185-188, 1991.

8. W. Huber, et al., "Direct Optical Immunosensing (Sensitivity and Selectivity)", *Sensors and Actuators,* vol.B6, p122-126, 1992.

9. A. Naumaan, J. T. Boyd, "Ring Resonator Fabrication in Phosphosilicate Glass Films Deposited by Chemical Vapor Deposition", *Journal of Lightwave Technology,* Vol.LT-4, No.9, p1294-1302, Sep., 1986.

10. M. Ohring, *The Materials Science of Thin Films*, Academic Press, New York, 1992.

11. W. Kern, R. S. Rosler, "Advances in Deposition Process", *J.Vac.Technol.,* Vol.14, No.5, p1072-2001, Sep./Oct., 1977.

12. A. C. Adams, C. D. Capio, "The Deposition of Silicon Dioxide Films at Reduced Pressure", *J.Electrochem.Soc.:Solid-State Science and Technology*, Vol.126, No.6, p1042-1046, 1979.

13. R. S. Rosler, "Low Pressure CVD Production Processes for Poly, Nitride, and Oxide", *Solid State Technology.*, Vol.20, p63, 1977.

14. M. Hammond and R. Gieske, Presented at *Semicon West*, Santa Clara, CA, May 27, 1976.

15. G. L. Schnable, W. Kern, and R. B. Comizzoli, "Passivation Coating on Silicon Devices", *J.Electrochem.Soc.:Solid-State Science and Technology*, Vol.122, No.8, p1092, August, 1993.

16. W. Kern, G. L. Schnable, and A. W. Fisher, *RCA Review*, Vol.37, p3, 1976.

17. J. Wong, "Low Pressure Deposition of Silicon Dioxide", *J.Electronic Mater.*, Vol.5, p113, 1977.

18. W. Kern, *Solid State Technology*, Vol.18, No.12, p25, 1976

19. B. J. Baliga and S. K.Ghandhi, "Growth of silica and Phosphosilicate Films", *J.Appl. Phys.*, Vol.44, No.3, p990, 1973.

20. J. Sandor, *ElectroChem. Soc. Ext. Abst.*, No.96, p228, 1962.

21. W. Kern, "Surface Passivation Techniques for Compound Solid State Devices", *Technical Report* No. AFAL-TR-65-213, Air Force Syst. Command, Wright-Patterson Air Force Base, OH, p1-13, August, 1965.

22. J. Oroshnik and J. Kraitchman, *J.Electrochem.Soc.:Solid-State Science and Technology,* Vol.115, p649, 1968.

23. W. Kern and J. P. White, *RCA Review*, Vol.31, p771, 1970.

24. E. Tanikawa, O. Takayama, and K. Maeda, in "Chemical Vapor Deposition, Fourth International Conference", G.F.Wakefield and J.M.Blocher, Jr., Editors, p261, *The Electrochemical society Softbound Proceedings Series*, Princeton, NJ, 1973.

25. K. Sugawara, T. Yoshimi, and H. Sakai, in "Chemical Vapor Deposition, Fifth International Conference", J.M.Blocher, Jr., H.E.Hintermann, and L.H.Hall, Editors, p407, *The Electrochemical society Softbound Proceedings* Series, Princeton, NJ, 1975.

26. S. Wolf and R. N. Tauber, *Silicon Processing for the VLSI Era,* Vol.1-Process Technology, Lattice Press, Sunset Beach, CA, 1986.

27. T. Y. Tien and F. A. Hummel, *J.AM.Ceram.Soc.*, Vol.45, p422, 1962.

28. J. M. Eldridge and P. Balk, *Trans.Met.Soc.AIME*, Vol.242, p539, 1968.

29. N. Nagasima, H. Suzuki, K. Tanaka, and S. Nishida, *J.Electronchem.Soc.:Solid-State Science and Technology,* Vol.121, No.3, p434, 1974.

30. N. Nagasima, *J.Appl.Phys.,* Vol.43, p3378, 1972.

31. W. A. Pliskin and H. S. Lehman, *J.Electrochem.Soc.:Solid-State Science and Technology*, Vol.112, p1013, 1965.

32. R. A. Levy, S. M. Vincent, and T. E. McGahan, , *J.Electronchem.Soc.:Solid-State Science and Technology*, Vol.132, No.6, p1472, 1985.

33. R. A. Levy and K. Nassau, , *J.Electronchem.Soc.:Solid-State Science and Technology*, Vol.133, No.7, p1417, 1986.

34. J. W. Mayer and S. S. Lau, *Electronics Materials Science: For Integrated Circuits in Si and GaAs*, Macmillan, New York, 1990.

35. A. C. Adams and S. P. Murarka, *J.Electronchem.Soc.:Solid-State Science and Technology*, Vol.126, No.2, p334, 1979.

36. P. A. Barnes and D. P. Schinke, *Appl.Phys.Lett.*, Vol.30, p26, 1977.

37. R. Ulrich and R. Torge, *Appl.Opt.*, Vol.12, p2901, 1973.

38. P. DuRant, in "Chemical Vapor Deposition, Fifth International Conference", J. M. Blocher, Jr., H. E. Hintermann, and L. H. Hall, Editors, p421, *The Electrochemical society Softbound Proceedings Series,* Princeton, NJ, 1975.

39. W. A. Plison and R. P. Gnall, *J.Electronchem.Soc.:Solid-State Science and Technology*, Vol.111, p872, 1964.

40. C. L. Luke, *Anal.Chim.Acta*, Vol.41, p237, 1968.

41. A. S. Tenny, and M. Ghezzo, , *J.Electronchem.Soc.:Solid-State Science and Technology*, Vol.120,No.9, p1276, 1973.

42. J. E. Franke, L. Zhang, and T. M. Niemczyk, , *J.Electronchem.Soc.:Solid-State Science and Technology*, Vol.140, No.5, p1425, 1993.

43. D. M. Haland, in *Computer-Enhanced Analytical Spectroscopy*, Vol.3, Peter C.Jurs, Editor, p1, Plenum Press, New York, 1992.

44. S. J. Lee, *Synthesis and characterization of Silicon Dioxide Thin Films By LPCVD Using Ditertiarybutylsilane and Oxygen*, MS.Thesis, Oct.1996, New Jersey Institute of Technology, Newark, NJ.

45. Vijiyalashmi Venkatesan, *Synthesis and Characterization of Silicon Dioxide and PSG Thin Films*, MS.Thesis, Oct.1996, New Jersey Institute of Technology, Newark, NJ.

46. R. M. Levin and A. C. Adams, *J.Electronchem.Soc.:Solid-State Science and Technology*, Vol.129, No.7, p1588, 1982.

47. G. Wahl, in "Chemical Vapor Deposition, Fifth International Conference", J.M.Blocher, Jr., H. E. Hintermann, and L. H. Hall, Editors, p19, *The Electrochemical society Softbound Proceedings Series*, Princeton, NJ, 1975.

48. W. Pliskin, and H. Lehman, *J.Electronchem.Soc.:Solid-State Science and Technology*, Vol.112, No.5, p11013, 1965.

49. W. Pliskin, *J.Vac.Sci.Technol.*, Vol.14, p1064, 1977.